INTERNATIONAL JOURNAL FOR NUMERICAL METHODS IN FLUIDS, VOL. 7, 409–452 (1987)

WAVE PROPAGATION ANALYSIS OF DIFFERENCE SCHEMES FOR HYPERBOLIC EQUATIONS: A REVIEW

ROBERT VICHNEVETSKY*

Department of Computer Science, Rutgers University, New Brunswick, N. J. 08903, U.S.A.

to r.

SUMMARY

There are spurious phenomena in the numerical approximation of the hyperbolic equations of fluid dynamics that may be investigated by invoking concepts which originate from wave propagation theory. Many of the significant results which have been obtained by pursuing this kind of analysis are reviewed in this paper by using as an illustration a family of implicit approximations of the simple linear advection equation. Included in this family of algorithms are the common six-point implicit finite difference scheme, the linear finite element/Galerkin scheme and the 'box' method.

The phase and group velocities of sinusoidal solutions are brought into the analysis of the accuracy and of the spurious reflection or scattering phenomena which are created at computational boundaries and in non-uniform grids. General properties become apparent in this Fourier/wave propagation approach to the analysis. One of these is in the form of an analogy with quantum mechanics. Another shows that certain energy norms of the errors are independent of time discretization, i.e. depend on space discretization alone.

KEY WORDS Numerical Analysis Finite Difference Schemes Hyperbolic Equations Wave Propagation Group Velocity Pure Advection Spurious Solutions

CONTENTS

*The research reported in this paper was carried out while the author was on a visiting appointment with Princeton University

0271–2091/87/050409–44$22.00

Received 12 March 1986
Revised 21 July 1986

INTRODUCTION

Many spurious phenomena in the numerical approximation of the hyperbolic equations of fluid dynamics may be explained by invoking concepts which originate from wave propagation theory. The purpose of this paper is to illustrate this by using as an example a family of implicit algorithms which have in common the fact that they are conservative and that they use a central finite difference approximation to the spatial derivatives. Included in this family of algorithms is the common six-point implicit finite difference scheme, a linear finite elements/Galerkin scheme and the so-called 'box' or 'quad' scheme.

Conservative wave propagation in a dispersive medium may be characterized by its phase velocity and its group velocity. Both concepts are needed in the analysis of wave propagation in numerical fluid dynamics: knowledge of the distortion in the phase velocity introduced by the approximation is sufficient to express the global error in the numerical solution of the Cauchy problem. On the other hand, the group velocity and the attending concept of energy propagation play an essential role in the analysis of parasitic reflection phenomena which manifest themselves at computational boundaries and at interior points of non-uniform grids.

It is in the investigation of these parasitic reflection phenomena that the wave propagation viewpoint takes its full power in the analysis of numerical algorithms for hyperbolic equations. Simple Fourier analysis of the numerical approximation of the pure initial value (or Cauchy) problem on a regular mesh has been well understood. It was first used by von Neumann who, in the 1940s, brought into numerical analysis the concept of 'sinusoidal trial solution', that was well known to fluid dynamicists as a means of testing the stability of flows;[1] von Neumann's use of this tool to test the stability of numerical approximations of the initial value problem was subsequently extended by others to investigate questions of accuracy as well.[2-11] But it is more recently (with a few exceptions) that the wave propagation, group velocity and energy flow concepts which are accessible through Fourier analysis have been recognized as a means of investigating the more difficult questions associated with boundaries and irregular grids. Typical contributions to this line of investigation may be found in References 12–25.

This review paper consists of two parts. In the first part (ending with section 10) the nature of numerical solutions in response to specified initial/boundary data is examined from the wave propagation viewpoint. In the second part (sections 11–16) those results are applied to the analysis of a number of spurious reflection phenomena which occur at boundaries and, in the case of non-uniform grids, at interior points of the computing domain.

Reviews give an opportunity to bring to the fore general properties and principles which may transcend the mathematical details. A first property of this kind which emerges from the analysis is in the form of an analogy: error wave propagation in computational fluid dynamics and the motion of particles in quantum mechanics share similar mathematics, which materialize themselves in a number of similar phenomena (cf. sections 6, 11 and 15). Another general property is contained in an independence or invariance principle which says that, when measured with

appropriate energy norms, spurious reflection phenomena are independent of time discretization, i.e. depend on space discretization alone (see in particular section 13).

PART I. PROPAGATION PROPERTIES

1. PROBLEM STATEMENT AND NOTATIONS

We shall use as a model the simple hyperbolic (advection) equation:

$$\frac{\partial U}{\partial t} + c\frac{\partial U}{\partial x} = 0 \tag{1}$$

and its numerical approximation on the regular grid:

$$x_n = nh; n = 0, \pm 1, \pm 2, \ldots \tag{2}$$

The class of algorithms that will be considered is based on the 3-point semi-discretization:

$$\frac{\mathrm{d}}{\mathrm{d}t}\left(\frac{\beta}{2}u_{n-1} + (1-\beta)u_n + \frac{\beta}{2}u_{n+1}\right) = -\frac{c}{2h}(u_{n+1} - u_{n-1}), \tag{3}$$

where β is a free parameter and the u_n are approximations of U at the nodes:

$$u_n(t) \simeq U(x_n, t). \tag{4}$$

When $\beta \neq 0$, then (3) is an implicit semi-discretization (i.e. derivatives on the left hand side are not given explicitly). This may also be viewed as the algorithm which is obtained when $U(x,t)$ is approximated with linear finite elements:

$$U(x,t) \simeq \sum_n \phi_n(x)u_n(t) \equiv u(x,t), \tag{5a}$$

$$\phi_n(x) = \begin{cases} 1 - \left|\dfrac{x - x_n}{h}\right|, & \text{when} \quad |x - x_n| \leqslant h, \\ 0, & \text{otherwise,} \end{cases} \tag{5b}$$

together with a method of weighted residuals with weights $g_n(x)$:

$$g_n(x) = \begin{cases} 1, & \text{when} \quad |x - x_n| \leqslant 2\beta h \\ 0, & \text{otherwise.} \end{cases} \tag{6}$$

The conditions

$$\langle \mathscr{R}, g_n \rangle \equiv \int \mathscr{R} g_n(x)\,\mathrm{d}x = 0, \tag{7a}$$

$$\mathscr{R} \equiv \frac{\partial u}{\partial t} + c\frac{\partial u}{\partial x} \tag{7b}$$

then result precisely in the system of equations (3). When $\beta = 0$, then (3) is the simple central finite difference approximation of (1); when $\beta = 1/3$, then (3) is the semi-discretization obtained with the linear finite elements/Galerkin method; and when $\beta = 1/2$, then (3) is what is called the 'box' or 'quad' method. Moreover, the finite difference case ($\beta = 0$) may be considered as the 'lumped mass' version of the finite element case ($\beta = 1/3$).[26]

The box scheme is a singular member of this family of algorithms and has distinctively unique properties. As will be seen, analysing this scheme within the broader context of a class of methods provides an insight into those unique properties which could not be otherwise obtained.

Full discretizations of the equation are obtained when a discrete stepping method is applied to the integration in time. The one we shall attach our attention to is the Crank–Nicolson method, but our results will have obvious applicability to other cases. For convenience, we rewrite (3) as

$$A_1 \frac{du_n}{dt} = A_2 u_n \tag{8}$$

where A_1 and A_2 are the operators

$$A_1 = 1 - \beta + \frac{\beta}{2}(E^{-1} + E),$$

$$A_2 = -\frac{c}{2h}(E - E^{-1}) \tag{9}$$

and E is the space shift operator defined by

$$u_{n+1} \equiv E u_n. \tag{10}$$

The Crank–Nicolson time stepping method may then be expressed as

$$A_1\left(\frac{u_n^{j+1} - u_n^j}{\Delta t}\right) = \frac{A_2}{2}(u_n^j + u_n^{j+1}),$$
$$u_n^j \simeq U(x_n, j\Delta t), \tag{11}$$

or, in operator form

$$M(Z)u_n^j = A(E)u_n^j. \tag{12}$$

Here, M and A are the operators

$$A(E) = A_1^{-1}(E)A_2(E), \tag{13}$$

$$M(Z) = \frac{2}{\Delta t}\frac{Z-1}{Z+1} \tag{14}$$

and Z is the time shift operator, defined by

$$u_n^{j+1} \equiv Z u_n^j. \tag{15}$$

The procedure which consists of approximating spatial derivatives at first and then applying consistently a time stepping algorithm to the resulting semi-discretization is sometimes called a 'method of lines' after Russian authors who coined this term in the 1940s (see also Reference 27).

The simple first order equations (1), (3) and (12) are of course meant to be models of hyperbolic systems of an order greater than one (typically the equations of fluid dynamics) and of their numerical approximation, to be used for the analysis of the behaviour of errors. It is indeed the case that errors, which may be viewed as small perturbations superimposed on the solutions of these systems, are described locally by linear equations which, when written in their characteristic form, consist of several first order independent equations of the kind used in these models. Several of the results derived in this paper will coincide in specific cases with similar results obtained with linearized models of the shallow water equations, for example by Chu and Sereny,[13] Foreman[6,15] and Cathers and O'Connor.[3]

2. FOURIER ANALYSIS

Equation (1) admits sinusoidal solutions of the form

$$U = e^{i(\omega t + \xi x)}, \tag{16}$$

where the frequency ω and the wave number ξ are related by

$$\omega = -c\xi. \tag{17}$$

The linearity of this relation expresses the lack of dispersion in the solutions of that equation. But this does not remain true for solutions of the numerical approximations (3) or (12). Their dispersion relations (the relations which replace (17) in these cases) are no longer linear. They are derived by inserting a sinusoidal trial solution in the equation and seeking the relation between ω and ξ that must be satisfied. For instance, in the fully discrete case (12) we choose the trial solution

$$u_n^j = e^{i(\omega j\Delta t + \xi nh)}. \tag{18}$$

The Fourier symbols of the operators A and M are defined as

$$i\alpha(\xi) \equiv Ae^{i\xi nh}/e^{i\xi nh} = A(e^{i\xi h}) \tag{19}$$

and

$$i\mu(\omega) \equiv Me^{i\omega j\Delta t}/e^{i\omega j\Delta t} = M(e^{i\omega\Delta t}), \tag{20}$$

respectively. A search for the condition under which the trial solution (18) satisfies (12) then results simply in

$$\mu(\omega) = \alpha(\xi) \tag{21}$$

or

$$\frac{2}{\Delta t}\tan\left(\frac{\omega\Delta t}{2}\right) = -\frac{c}{h}\left(\frac{\sin(\xi h)}{1-\beta+\beta\cos(\xi h)}\right), \tag{22}$$

which is the dispersion relation for (12). This relation is illustrated in Figure 1, where the abscissa is also labelled with the wavelength

$$\lambda = 2\pi/\xi \tag{23}$$

as an alternative independent variable. The analysis is meaningful only when $|\xi| \leqslant \pi/h$ (or $\lambda \geqslant 2h$), which is an expression of the sampling theorem.[28,29]

When we let $\Delta t \to 0$, then the full discretization (12) becomes the semi-discretization (3) and (22) becomes

$$\omega = -\frac{c}{h}\left(\frac{\sin(\xi h)}{1-\beta+\beta\cos(\xi h)}\right), \tag{24}$$

which is the corresponding form of the dispersion relation.

The phase velocity is defined by

$$c^* = -\frac{\omega}{\xi}, \tag{25}$$

which gives, with (22),

$$c^* = c\frac{2}{\xi hR}\arctan\left[\frac{R}{2}\left(\frac{\sin(\xi h)}{1-\beta+\beta\cos(\xi h)}\right)\right] \tag{26}$$

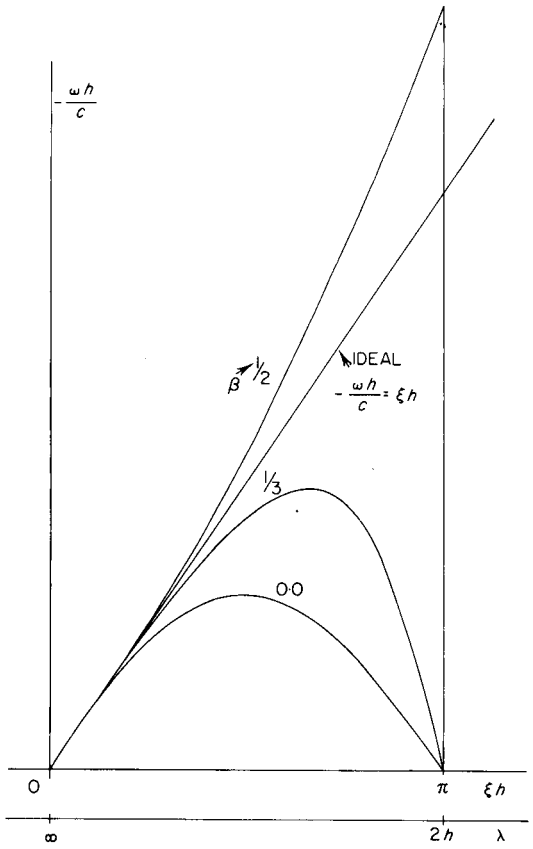

Figure 1. Dispersion relation for the finite difference ($\beta = 0$), finite element ($\beta = 1/3$) and box ($\beta = 1/2$) methods. $R(\equiv c\Delta t/h) = 0{\cdot}75$

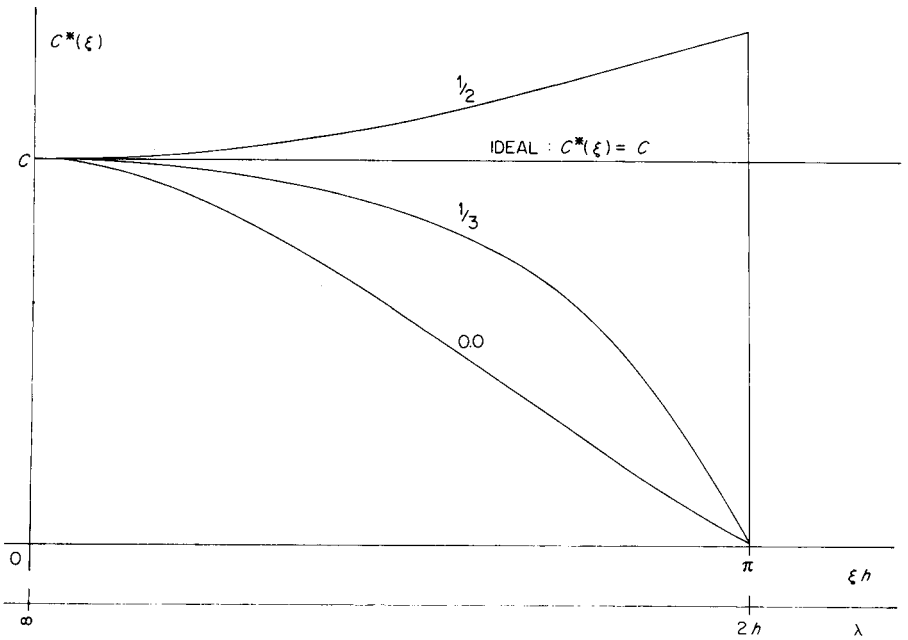

Figure 2. Phase velocities for the finite difference ($\beta = 0$), finite element ($\beta = 1/3$) and box ($\beta = 1/2$) methods—the same cases as those given in Figure 1

(Figure 2), where

$$R \equiv \left| \frac{c\Delta t}{h} \right| \tag{27}$$

is the Courant number. In the semi-discrete case ($R \to 0$) then c^* becomes

$$c^* = \frac{c}{\xi h}\left(\frac{\sin(\xi h)}{1 - \beta + \beta\cos(\xi h)} \right). \tag{28}$$

as may be noted, the phase velocity of the numerical solution is always non-negative. This will stand in contrast with group velocities: it will be seen in section 5 that the group velocities of solutions of this family of algorithms may assume both positive and negative signs.

3. ENERGY CONSERVATION

If we multiply (3) by $2hu_n$ and sum over $n \in (-\infty, \infty)$, then we find, for $\{u_n\}$ of finite l_2 norm:

$$\frac{\mathrm{d}}{\mathrm{d}t} h \sum_n u_n \left[(1-\beta)u_n + \frac{\beta}{2}(u_{n-1} + u_{n+1}) \right] = 0. \tag{29}$$

This defines

$$\mathscr{E}_\beta(t) = h \sum_n u_n \left[(1-\beta)u_n + \frac{\beta}{2}(u_{n-1} + u_{n+1}) \right] \tag{30}$$

as a quantity which is conserved by solutions of the Cauchy problem for the semi-discretization (3). We shall, in the present context, call $\mathscr{E}_\beta$ the energy (or natural energy) of $\{u_n\}$. Its expression in Fourier space is the modified form of Parseval's relation:[29]

$$\mathscr{E}_\beta(t) = \int_{-\pi/h}^{\pi/h} |\bar{u}(\xi, t)|^2 w(\xi) \frac{\mathrm{d}\xi}{2\pi}, \tag{31a}$$

where $w(\xi)$ is the weight function:

$$w(\xi) = 1 - \beta + \beta\cos(\xi h) \tag{31b}$$

and $\bar{u}(\xi, t)$ is the discrete x-Fourier transform of $\{u_n(t)\}$:

$$\bar{u}(\xi, t) \equiv h \sum_{n=-\infty}^{\infty} u_n(t) \mathrm{e}^{-\mathrm{i}\xi n h}. \tag{32}$$

The inverse of $\bar{u}(\xi, t)$ is

$$u_n(t) = \int_{-\pi/h}^{\pi/h} \bar{u}(\xi, t) \mathrm{e}^{\mathrm{i}\xi n h} \frac{\mathrm{d}\xi}{2\pi}. \tag{33}$$

We may verify that when $\beta \leqslant \frac{1}{2}$, $w(\xi)$ cannot be negative. With (31a), this shows that $\mathscr{E}_\beta$ is also always non-negative, as should be expected of an energy-like quantity.

The integrand of (31a):

$$|\bar{u}(\xi, t)|^2 w(\xi) \tag{34}$$

is the spectral distribution of the energy of u. It is easily verified that this energy distribution function is invariant with respect to time:

$$|\bar{u}(\xi,t)|^2 w(\xi) = |\bar{u}(\xi,0)|^2 w(\xi). \tag{35}$$

The distribution of energy in physical space:

$$hu_n\left[(1-\beta)u_n + \frac{\beta}{2}(u_{n-1}+u_{n+1})\right] \tag{36}$$

is of course time dependent.

It could be argued that not only is (30) invariant with respect to time, but that so also is the square of the l_2 norm of u (which we shall call the l_2 energy of u in the present context):

$$\|u_n\|_2^2 \equiv h\sum_{n=-\infty}^{\infty}|u_n|^2 = \int_{-\pi/h}^{\pi/h}|\bar{u}(\xi,t)|^2\frac{\mathrm{d}\xi}{2\pi}. \tag{37}$$

But when the analysis is extended to include irregular grids (i.e. when h is no longer a constant), then the corresponding form of (30) remains invariant, whereas that of (37) does not (see sections 11 and 14 below). Because of its invariance property, $\mathscr{E}_\beta$ is a more appropriate measure than (37) to be used in the analysis of reflection or scattering at mesh variation interfaces and boundaries. The l_2 energy is however also of practical interest. It is this quantity (and not $\mathscr{E}_\beta$) which measures what users call 'spurious noise' in a given computation. (The l_2 and natural energies are identical in the finite difference, $\beta = 0$, case.)

The same form of invariant energy applies to the fully discrete case. To show that this is so, we multiply equation (11) by $h\Delta t(u_n^{j+1} + u_n^j)$ and sum over all n to obtain simply

$$\mathscr{E}_\beta^{j+1} - \mathscr{E}_\beta^j = 0, \tag{38}$$

which is the discrete time analogue of (29) which applies to solutions of the Cauchy problem for (11).

When dealing with finite domains, then the corresponding definition (30) for the energy contains a finite instead of an infinite sum. The energy conservation principles (29) and (38) become

$$\frac{\mathrm{d}\mathscr{E}_\beta}{\mathrm{d}t} = \text{boundary terms} \tag{39}$$

and

$$\mathscr{E}_\beta^{j+1} - \mathscr{E}_\beta^j = \text{boundary terms}. \tag{40}$$

It is to be noted that these principles merely reflect the preservation of similar principles that apply to true solutions of (1). Solutions of that equation satisfy

$$\frac{\mathrm{d}}{\mathrm{d}t}\int_{-\infty}^{\infty}[U(x,t)]^2\,\mathrm{d}x = 0 \tag{41}$$

when $U(x,t)$ belongs to a Hilbert space and the computing domain D is the entire real axis; (39) and (40) are the analogues of

$$\frac{\mathrm{d}}{\mathrm{d}t}\int_A^B[U(x,t)]^2\,\mathrm{d}x = -c[U(A,t)^2 - U(B,t)^2] \tag{42}$$

when D is finite.

Some comments are in order: 'trial solutions' of the form (18) are not of finite l_2 norm and they do not formally have Fourier transforms. By contrast, the solutions considered in the present section are of finite l_2 norm (they belong to a Hilbert space); they can be Fourier transformed, and Fourier analysis applies with all its power, including in particular the quantification of the magnitude of solutions with energy norms expressed by integrals of the forms (31)–(37).

4. ANALYSIS WITH t-FOURIER TRANSFORMS

We have, in the preceding sections, introduced x-Fourier transforms into the analysis. Wave propagation may also be analysed with t-Fourier transforms. This will turn out to be the appropriate tool for the description of scattering or reflection at boundaries and mesh refinement interfaces. (Relevant comments on those new aspects of wave propagation which are revealed when the frequency ω is introduced into the analysis—as is the case when one uses t-Fourier transforms—may be found in Brillouin's reference to Lord Kelvin's work on light propagation in crystals (Reference 30, p. 5).

The discrete t-Fourier transform of $\{u_n\}$ is defined as

$$\bar{u}_n(\omega) = \Delta t \sum_{j=-\infty}^{\infty} u_n^j e^{-i\omega j\Delta t}. \tag{43}$$

Its inverse is

$$u_n^j = \int_{-\pi/\Delta t}^{\pi/\Delta t} \bar{u}_n(\omega) e^{i\omega j\Delta t} \frac{d\omega}{2\pi}. \tag{44}$$

Taking the discrete t-Fourier transform of equation (12) results in

$$\left(\frac{1}{2} + i\frac{\beta}{2}\frac{\mu h}{c}\right)\bar{u}_{n+1} + (1-\beta)i\frac{\mu h}{c}u_n - \left(\frac{1}{2} - i\frac{\beta}{2}\frac{\mu h}{c}\right)\bar{u}_{n-1} = 0. \tag{45}$$

This equation may be solved analytically by seeking normal solutions, i.e. solutions for which the ratio

$$\frac{\bar{u}_{n+1}(\omega)}{\bar{u}_n(u)} \equiv \hat{E}(\omega) \tag{46}$$

is independent of n. Inserting this in (45) results in the characteristic equation

$$\left(\frac{1}{2} + i\frac{\beta}{2}\frac{\mu h}{c}\right)\hat{E}^2 + (1-\beta)i\frac{\mu h}{c}\hat{E} - \left(\frac{1}{2} - i\frac{\beta}{2}\frac{\mu h}{c}\right) = 0 \tag{47}$$

for $\hat{E}$. This equation has the two roots

$$\hat{E}(\omega) = \frac{-i(1-\beta)\bar{\mu} \pm \sqrt{[1-(1-2\beta)\bar{\mu}^2]}}{1+i\beta\bar{\mu}}, \tag{48a}$$

where $\bar{\mu}$ is the dimensionless quantity

$$\bar{\mu}(\omega) = \mu(\omega)\frac{h}{c}. \tag{48b}$$

Equation (45) thus admits two types of solutions, which satisfy

$$\frac{\bar{p}_{n+1}(\omega)}{\bar{p}_n(\omega)} = \frac{-i(1-\beta)\bar{\mu} + \sqrt{[1-(1-2\beta)\bar{\mu}^2]}}{1+i\beta\bar{\mu}} \equiv \hat{E}_p(\omega) \tag{49}$$

and

$$\frac{\bar{q}_{n+1}(\omega)}{\bar{q}_n(\omega)} = \frac{-i(1-\beta)\bar{\mu} - \sqrt{[1-(1-2\beta)\bar{\mu}^2]}}{1+i\beta\bar{\mu}} \equiv \hat{E}_q(\omega), \tag{50}$$

respectively. It will found later on in the analysis that solutions which satisfy (49)—which we shall call solutions of p type—are, when $\omega \to 0$, consistent approximations of genuine solutions of the problem at hand, whereas solutions which satisfy (50)—which we shall call solutions of q type—are entirely spurious.

It is easily verified that for values of ω which satisfy the equation

$$|\mu(\omega)| \leqslant \mu(\omega_c) = \frac{c}{h\sqrt{(1-2\beta)}} \tag{51}$$

(where ω_c is defined as the cut-off frequency), we have

$$|\hat{E}_p(\omega)| = |\hat{E}_q(\omega)| = 1, \tag{52}$$

i.e.

$$|\omega| \leqslant \omega_c \tag{53}$$

is the frequency band in which constant amplitude wave propagation may exist. As we shall see, solutions of p and q type are characterized, in that band, by rightgoing and leftgoing wave propagation, as described by their respective group velocities. This will be examined in the next section.

When $|\omega| > \omega_c$, then solutions which are sinusoidal in time may still exist, but they cannot have a constant amplitude in space; these are the 'evanescent solutions' that will be analysed in section 9.

The explicit form of the cut-off frequency obtained by solving (51) is (Figure 3)

$$\omega_c = \frac{2}{\Delta t}\arctan\left(\frac{R}{2}\frac{1}{\sqrt{(1-2\beta)}}\right), \tag{54}$$

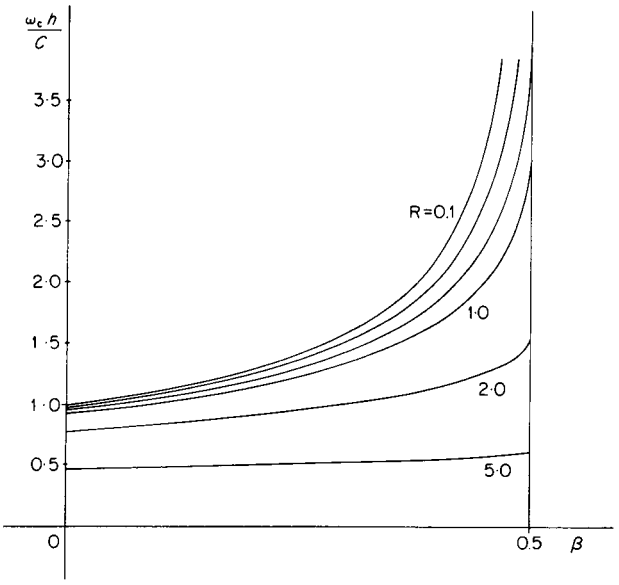

Figure 3. Cut-off frequency versus the parameter β for Courant numbers $R = 0{\cdot}1, 0{\cdot}5, 0{\cdot}75, 1, 2$ and 5. For large values of R, the cut-off frequency approaches that introduced by the time discretization alone, which is $\omega_{c,\Delta t} = \pi/\Delta t$ or $\omega_{c,\Delta t h}/c = \pi/R$

which becomes, in the semi-discrete case ($R \to 0$),

$$\omega_c = \frac{c}{h} \frac{1}{\sqrt{(1-2\beta)}}. \tag{55}$$

Of particular interest is the case $\beta = 1/2$ (the box method). The cut-off frequency (54) is then

$$\omega_c = \frac{\pi}{\Delta t}, \tag{56}$$

which is half the sampling frequency of the time discretization, and is independent of the space discretization step h. The expressions of (49) and (50) become

$$\hat{E}_p(\omega) = \frac{1 - i\bar{\mu}/2}{1 + i\bar{\mu}/2} \tag{57}$$

and

$$\hat{E}_q(\omega) = -1. \tag{58}$$

The fact that the relationship between μ and $\hat{E}$ is rational indicates that the 3-point algorithm (12) may in this case be decomposed into two 2-point algorithms which admit (57) and (58) as their respective solutions.

Indeed, it may be verified that (57) and (58) also describe the solutions of

$$M\left(\frac{p_{n+1} + p_n}{2}\right) = -\frac{c}{h}(p_{n+1} - p_n) \tag{59}$$

and

$$q_{n+1} = -q_n, \tag{60}$$

respectively. When M is the Crank–Nicolson operator, then (59) may also be written as

$$\frac{1}{\Delta t}[(p_{n+1}^{j+1} + p_n^{j+1}) - (p_{n+1}^{j} + p_n^{j})]$$

$$= -\frac{c}{h}[(p_{n+1}^{j+1} - p_n^{j+1}) + (p_{n+1}^{j} - p_n^{j})], \tag{61}$$

which is the usual form in which this method may be found in the literature.[31,32] No such decomposition is possible for other values of β.

5. GROUP VELOCITY

The group velocity is the velocity at which sinusoidal waves propagate energy in a dispersive medium.[30,33,52] Its expression is

$$G = -\frac{d\omega}{d\xi}, \tag{62}$$

where $\omega(\xi)$ is the dispersion relation. A first expression of the group velocity for solutions of (12) may be obtained with (22). We find

$$G = c\frac{\beta + (1-\beta)\cos(\xi h)}{[1 - \beta + \beta\cos(\xi h)]^2} \frac{d\omega}{d\mu}, \tag{63}$$

with (Crank–Nicolson case)

$$\frac{d\omega}{d\mu} = \cos^2\left(\frac{\omega\Delta t}{2}\right)$$

$$= \frac{[1-\beta+\beta\cos(\xi h)]^2}{[1-\beta+\beta\cos(\xi h)]^2 + \left[\frac{R}{2}\sin(\xi h)\right]^2}. \tag{64}$$

This gives (Figure 4)

$$G(\xi) = c\frac{\beta+(1-\beta)\cos(\xi h)}{[1-\beta+\beta\cos(\xi h)]^2 + \left[\frac{R}{2}\sin(\xi h)\right]^2}. \tag{65}$$

The expression of the group velocity G as a function of the frequency ω may be obtained by making use of the evident identity

$$\hat{E}(\omega) = e^{i\xi h}, \tag{66}$$

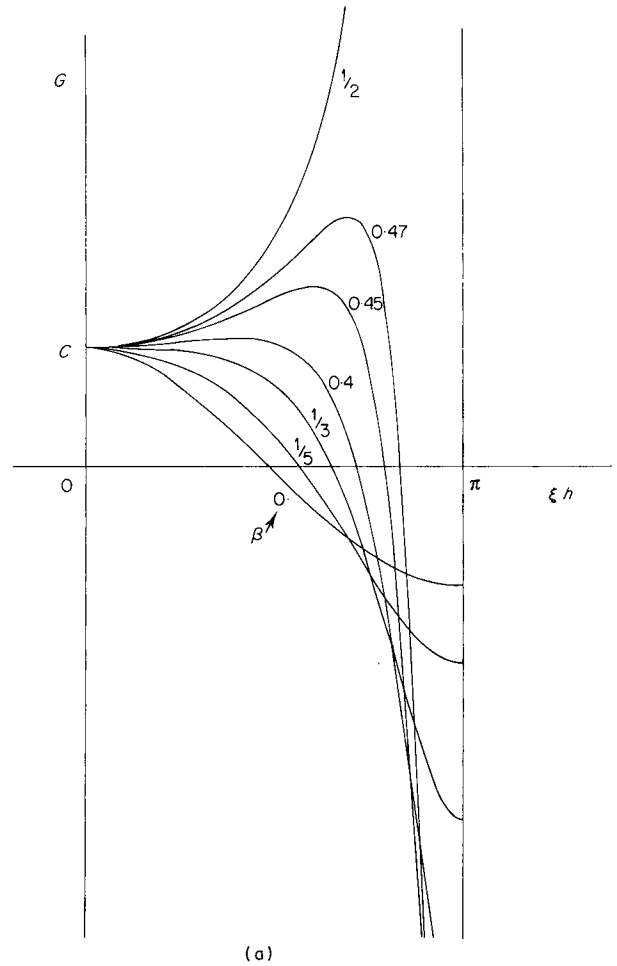

Figure 4(a). Group velocity versus wavenumber for $\beta = 0, 1/5, 1/3, 0{\cdot}4, 0{\cdot}45, 0{\cdot}47$ and $1/2$. $R = 0.25$

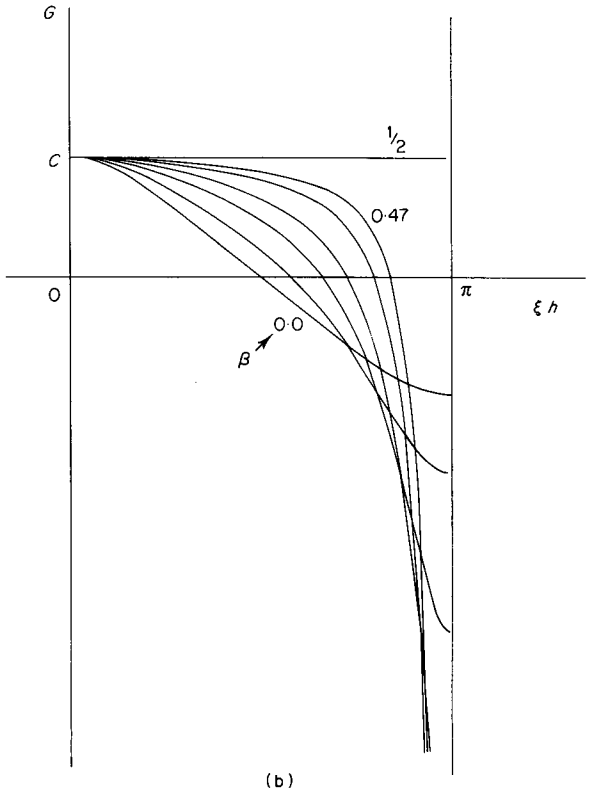

Figure 4(b). Group velocity versus wavenumber for $\beta = 0, 1/5, 1/3, 0{\cdot}4, 0{\cdot}45, 0{\cdot}47$ and $1/2$. $R = 1$

which is an operator form of the dispersion relation. From this results

$$\mathrm{Re}[\hat{E}(\omega)] = \cos(\xi h) \tag{67}$$

and, with (63) and (64),

$$G_p(\omega) = c\frac{\sqrt{[1-(1-2\beta)\bar{\mu}^2]}}{(1-\beta)+\beta\sqrt{[1-(1-2\beta)\bar{\mu}^2]}}(1+\beta^2\bar{\mu}^2)\cos^2\left(\frac{\omega\Delta t}{2}\right), \tag{68}$$

$$G_q(\omega) = -c\frac{\sqrt{[1-(1-2\beta)\bar{\mu}^2]}}{(1-\beta)-\beta\sqrt{[1-(1-2\beta)\bar{\mu}^2]}}(1+\beta^2\bar{\mu}^2)\cos^2\left(\frac{\omega\Delta t}{2}\right), \tag{69}$$

where the subscripts p and q refer to the two types of solutions defined by (49) and (50).

Important to note is the fact that G_p is always positive when $|\omega| < \omega_c$: solutions of p type are rightgoing. Moreover, G_p tends to c when $\omega h \to 0$. This is an expression of the consistency property of solutions of p type.

By contrast, G_q is always negative for the same frequencies, which makes solutions of q type leftgoing and spurious.

This deserves some comments: when one talks of leftgoing and rightgoing (sinusoidal) solutions, it is implied that one refers to the direction in which those solutions propagate energy, or wave packets. The corresponding velocity is the group velocity, not the phase velocity. It has been seen in section 2 that phase velocities are always non-negative. The observation of the fact that

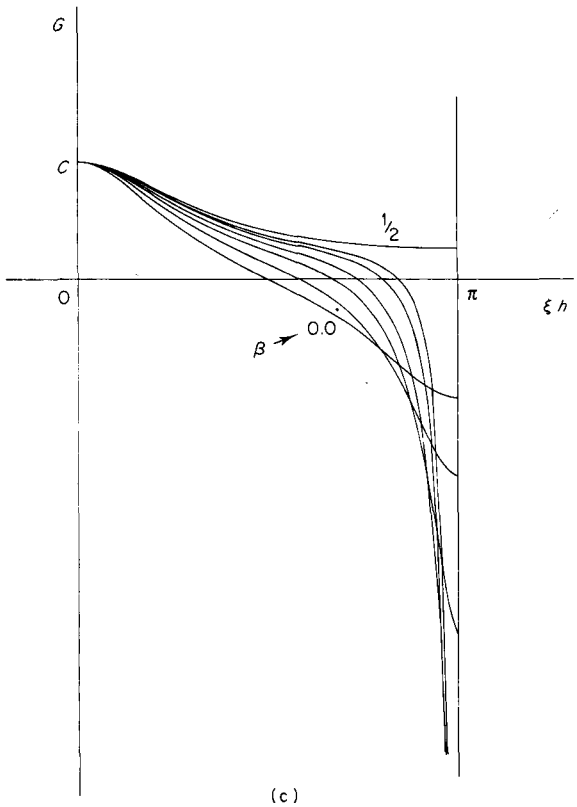

Figure 4(c). Group velocity versus wavenumber for $\beta = 0, 1/5, 1/3, 0{\cdot}4, 0{\cdot}45, 0{\cdot}47$ and $1/2$. $R = 2$

solutions of q type are leftgoing, and the analysis of reflection and related boundary phenomena to which this observation will lead, would be inaccessible with the use of phase velocities alone.

Since the group velocity is equal to minus the slope of the dispersion curve, it may be observed (for instance with Figure 1) that solutions of p type correspond to smaller wave numbers (or higher wavelengths extending upwards to $\lambda = \infty$), whereas solutions of q type correspond to higher wave numbers (or smaller wavelengths extending downwards to $\lambda = 2h$).

We note (Figure 4(a)) that when $\beta > 1/3$ and $R < 1$, then there are wave numbers in $|\xi h| \in (0, \pi)$ for which $G > c$. That the value $\beta = 1/3$ separates those cases which admit group velocities greater than c from those which do not is directly related to the fact that the corresponding method (the linear finite element/Galerkin method) gives the highest degree of consistency attainable with this family of algorithms, sometimes called the superconvergence property of the corresponding case.[34] A note of caution: this superconvergence property of the finite element method applies only to the case of regular grids ($h =$ constant) and is thus often lost. It is indeed frequently the case that non-equal elements, and in several dimensions non-rectangular elements, are used in practice.

That the discrete equation (12) admits two types of solutions results from the fact that this equation is of second order (whereas the original equation (1) is of the first order). If we let $|\omega \Delta t| \to 0$, then the dispersion relation (22) gives the two corresponding wave numbers:

$$|\xi h| \to 0; \quad |\xi h| \to \pi. \tag{70}$$

It may be shown independently that when $|\omega\Delta t| \to 0$, then (12) becomes the system

$$\frac{\partial P}{\partial t} + c\frac{\partial P}{\partial x} = 0, \tag{71a}$$

$$\frac{\partial Q}{\partial t} - c\left(\frac{1}{1-2\beta}\right)\frac{\partial Q}{\partial x} = 0, \tag{71b}$$

where P and Q are the analogues of solutions in $|\xi h| \to 0$ and $|\xi h| \to \pi$, respectively (References 29, p. 83; see also Figure 13 below), i.e. the numerical approximation (12) is consistent not only with the first order equation (1), but also with the second order system (71). And it is interesting to note that the characteristic velocities of that second order system are correspondingly related to the group velocities:

$$c = \lim_{\omega \to 0} G_p(\omega),$$

$$-c\left(\frac{1}{1-2\beta}\right) = \lim_{\omega \to 0} G_q(\omega). \tag{72}$$

In the particular case of the box method and $R < 1$, then G is monotonically increasing from

$$G(\xi h = 0) = c \tag{73}$$

towards its maximum value when $|\xi h| \to \pi$:

$$G(|\xi h| \to \pi) = \frac{c}{R^2}. \tag{74}$$

This describes solutions of p type, i.e. those which satisfy (57) and does not include the point $|\xi h| = \pi$. Solutions of q type are singular in this case: they correspond to the single wave-number $|\xi h| = \pi$ (or single wavelength $\lambda = 2h$). And by (69), their group velocity is infinite:

$$G_q(|\xi h| = \pi) = -\infty. \tag{75}$$

When the box method is implemented as the two-point formula (59) then, obviously, this type of solution does not exist. But it does exist with (12), $\beta = 1/2$. Illustrations of this type of solution will be given in section 16.

6. THE INITIAL VALUE (CAUCHY) PROBLEM

It has been shown in section 3 that the energy of $\{u_n\}$ (equation (30)) is invariant when $\{u_n\}$ is a solution of the Cauchy problem for (3) or (12). This implies numerical stability.

Keeping with the wave analysis viewpoint, an initial function

$$\{u_n^0\} \quad \text{imposed in} \quad D \equiv (-\infty, \infty) \tag{76}$$

may be considered as the superposition of Fourier components of different wave numbers. The separation in x-Fourier space between rightgoing and leftgoing solutions may be obtained by pursuing the analysis of section 5: the separating wave number ξ_c is that which corresponds to a zero group velocity. Equating (63) to zero results in (Figure 5)

$$\xi_c h = \arccos\left(\frac{\beta}{\beta - 1}\right), \tag{77}$$

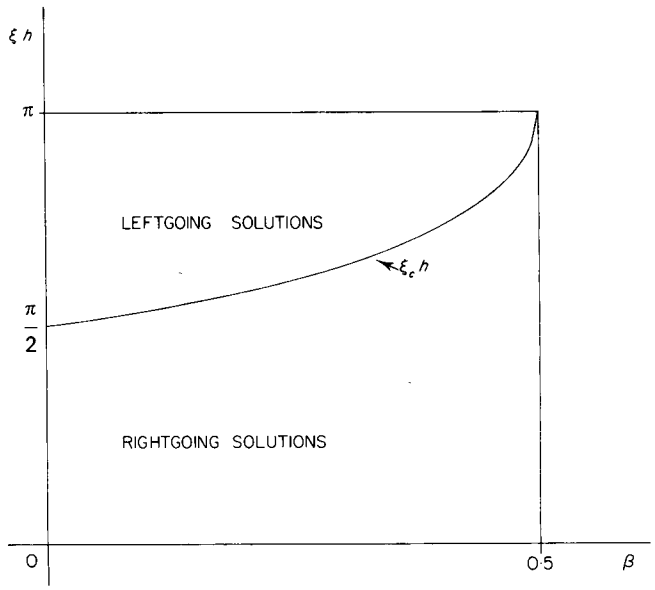

Figure 5.

which is independent of the Courant number R. And ξ_c is obviously related to ω_c (equation (54)) by the dispersion relation.

Fourier components of u^0 are thus separated into rightgoing components (of p type) for

$$0 \leqslant |\xi h| < \xi_c h \tag{78a}$$

and leftgoing components (of q type) for

$$\xi_c h < |\xi h| \leqslant \pi. \tag{78b}$$

Numerical experiments with wave packets

Single, monochromatic sinusoidal functions (or Fourier components) extend formally from $-\infty$ to $+\infty$ and they cannot be used to conduct meaningful numerical experiments, which are necessarily in finite domains: a natural procedure for the implementation of such experiments consists of using wave packets (also called wave groups). The classical definition of a wave packet is given, somewhat heuristically as: 'a sinusoidal function of finite length, comprising only a limited number of wavelengths' (a good expositions of these concepts may be found for instance in Reference 30). A convenient form of expression for such wave packets (to be used for the generation of initial data) is that of a sinusoidal function with a Gaussian envelope of standard deviation σ:

$$U(x,0) = \mathrm{e}^{-(1/2)[(x-x_0)/\sigma]^2} \mathrm{e}^{i\xi_0 x}. \tag{79a}$$

Its Fourier transform also has a Gaussian envelope, of standard deviation $1/\sigma$:

$$|\hat{U}_{(\xi,0)}| = \sqrt{2\pi}\, \mathrm{e}^{-1/2\,[(\xi-\xi_0)\sigma]^2}. \tag{79b}$$

But (79) is only the approximation of a wave packet: both (79a) and (79b) have infinite support. By contrast, an ideal wave packet should be of finite length in x and of vanishingly small wave number (and frequency) bandwidth.

It is, however, the case that the energy of (79) is concentrated, to within a negligible remainder, in a finite region near x_0 in physical space, and in a narrow wave number band near ξ_0 in Fourier space (the energy of (79a) which is contained outside of $(x_0 - 5\sigma, x_0 + 5\sigma)$ is of the order of 10^{-7} times the total energy, and likewise in Fourier space). The product of the approximate widths of the two corresponding distribution functions is of order one: this is an expression of what is known as the bandwidth theorem in Fourier analysis. Loosely stated, it says that this product is bounded from below by a number of order one for any function $U(x)$. Moreover, this lower bound is reached by Gaussians of the form (79a). One cannot create, for the purpose of conducting numerical experiments, ideal wave packets of finite support in physical space, and (79a) is the best approximation thereof one may get. When σ is reasonably large with respect to the wavelength $\lambda_0 = 2\pi/\xi_0$ then (79a) approximates a wave packet of wave number ξ_0.

This is no different from the situation in quantum mechanics where elementary particles and their associated wave trains are subjected to Heisenberg's uncertainty principle. This principle and the bandwidth theorem of Fourier analysis are essentially expressions of the same mathematics.[35] This is our first encounter with the analogy between numerical wave propagation and mathematical physics. Others will follow.

Given in Figure 6 are the results of numerical experiments which illustrate the difference in the wave propagation property of solutions of (12) for different values of β. The initial function

$$u_n^0 = \left[1 + \cos\left(\frac{\pi x_n}{h}\right)\right] e^{-0.5[(x-x_0)/\sigma]^2}, \quad (\sigma = 5)$$

imposed in D consists of two superimposed wave packets, one of which is a solution of p type with wave number satisfying $|\xi h| \to 0$ (or wavelength $\lambda \to \infty$), the other of which is a solution of q type (when $\beta \neq 1/2$) with $|\xi h| \to \pi$ (or $\lambda \to 2h$). The two wave packets move at the corresponding group velocities:

$$G(|\xi h| = 0) = c \tag{80a}$$

and

$$G(|\xi h| = \pi) = -\frac{c}{1 - 2\beta}. \tag{80b}$$

The band of wave numbers which correspond to leftgoing solutions decreases as β increases, and disappears when $\beta = 1/2$ (box method). Correspondingly, the saw-toothed wave packet of Figure 6(d) may be observed to be a solution of p type, and not of q type as it is for other values of β. Solutions of q type are restricted with the box method to the single point $|\xi h| = \pi$. We shall see in section 16 that it takes boundary conditions (as opposed to initial conditions) to generate those solutions.

Although group velocities are essential to the analysis of spurious reflection phenomena, it must be noted that they are not needed to express the error in numerical approximations of the Cauchy problem on a regular discretization of the x axis. To illustrate this, consider the scheme (12) on $x \in (-\infty, \infty)$ with the initial condition (76). The numerical solution may be expressed analytically as

$$u_n^i = \int_{-\pi/h}^{\pi/h} \overline{u}^0(\xi) e^{i\xi(x_n - c^*(\xi)t^j)} \frac{d\xi}{2\pi}, \tag{81}$$

where $\overline{u}^0(\xi)$ is the Fourier transform of $\{u_n^0\}$.

If $\hat{U}(\xi, 0)$ is band limited in $(-\pi/h, \pi/h)$, then there is no aliasing associated with the initial sampling (Reference 29 pp. 16–17) and

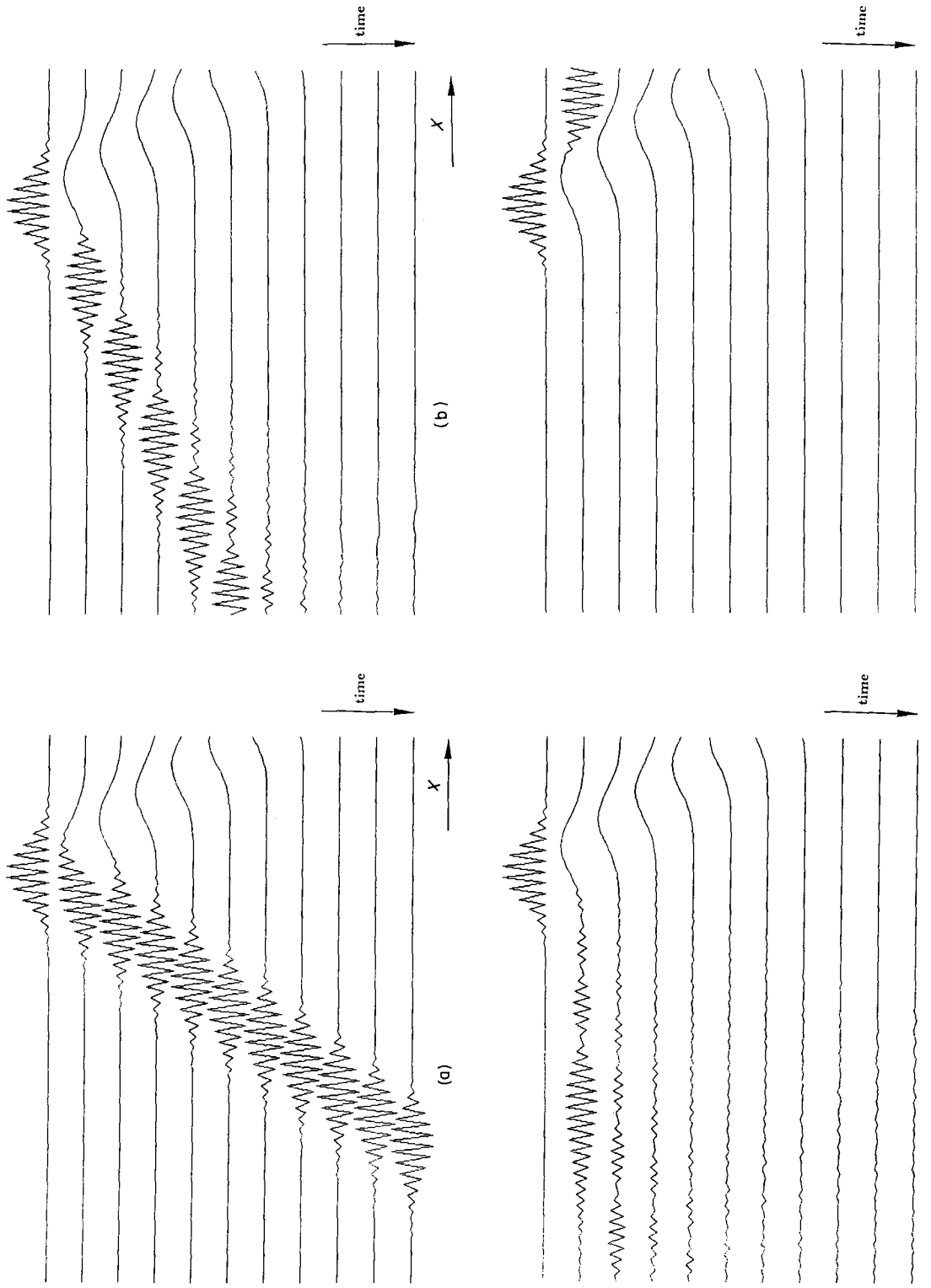

Figure 6. Superposition of two wave groups of wave numbers $|\xi h| \simeq 0$ and $|\xi h| \simeq \pi$, respectively. Courant number: $R = 0{\cdot}25$; $h = 1$. Except in the box case ($\beta = 0{\cdot}5$) the first wavegroup is of p type (rightgoing) and the second is of q type (leftgoing). In the box case, both are rightgoing. The absorbing boundary scheme (140) is used at the upwind boundary and the actual computing domain extends well beyond the figure to the right: (a) $\beta = 0$; (b) $\beta = 1/3$; (c) $\beta = 0{\cdot}45$; (d) $\beta = 0{\cdot}5$

$$\bar{u}^0(\xi) = \hat{U}(\xi, 0). \tag{82}$$

The true solution of this problem is then

$$U(x_n, t^j) = \int_{-\pi/h}^{\pi/h} \bar{u}^0(\xi) e^{i\xi(x_n - ct^j)} \frac{d\xi}{2\pi}. \tag{83}$$

This gives the following expression for the error:

$$u_n^j - U(x_n, t^j) = \int_{-\pi/h}^{\pi/h} \bar{u}^0(\xi) e^{i\xi x_n} (e^{-i\xi c^*(\xi) t^j} - e^{-i\xi c t^j}) \frac{d\xi}{2\pi}. \tag{84}$$

Its l_2 energy may be expressed by use of the discrete form of Parseval's relation:

$$\| u_n^j - U(x_n, t^j) \|_2^2 = \int_{-\pi/h}^{\pi/h} \left| \bar{u}^0(\xi) 2 \sin \left[\frac{\xi}{2} (c^*(\xi) - c) t^j \right] \right|^2 \frac{d\xi}{2\pi}, \tag{85}$$

which indeed depends on the algorithm used only through the phase velocity error

$$c^*(\xi) - c. \tag{86}$$

7. ENERGY FLOW AND CHARACTERISTIC IMPEDANCE

The total energy flow across a mesh point x_n is expressed by[36,52]

$$\mathscr{E}_{\beta,n} = \int_{-\omega_c}^{\omega_c} |u_n(\omega)|^2 w(\omega) G(\omega) \frac{d\omega}{2\pi}, \tag{87}$$

where the weight function $w(\omega)$ is derived from (31b) and the dispersion relation to replace ξ with ω. All calculations done, this results in

$$\mathscr{E}_{\beta,n} = \int_{-\omega_c}^{\omega_c} |u_n(\omega)|^2 W(\omega) \frac{d\omega}{2\pi}, \tag{88}$$

where $W(\omega)$ is

$$W(\omega) = \pm c \sqrt{[1 - (1 - 2\beta)\bar{\mu}^2]} \cos^2 \left(\frac{\omega \Delta t}{2} \right). \tag{89}$$

In classical wave propagation theory, this quantity is the real part of the characteristic admittance (or inverse of the characteristic impedance) of the medium and

$$\Phi_\beta(\omega) = |\bar{u}_n(\omega)|^2 W(\omega) \tag{90}$$

is the spectral distribution of the energy flow.

The function $W(\omega)$ may also be expressed simply as

$$W(\omega) = \pm c \sqrt{1 - [\mu(\omega)/\mu(\omega_c)]^2} \cos^2 \left(\frac{\omega \Delta t}{2} \right) \tag{91}$$

where ω_c is the cut-off frequency (54) and where the parameter β does not appear explicitly any more (it appears implicitly in ω_c which is a function of β).

Interesting to note is the fact that absolute value $|W(\omega)|$ is the same for leftgoing and rightgoing

solutions. By contrast, the flow of l_2 energy

$$\int_{-\omega_c}^{\omega_c} |\bar{u}_n(\omega)|^2 G(\omega) \frac{d\omega}{2\pi} \tag{92}$$

has the spectral distribution

$$\Phi_2(\omega) = |\bar{u}_n(\omega)|^2 G(\omega), \tag{93}$$

which has not, in general, the same property of symmetry, since

$$\left| \frac{G_q(\omega)}{G_p(\omega)} \right| > 1 \tag{94}$$

when $\beta \neq 0$.

We may also express W in terms of wave numbers:

$$\begin{aligned} W(\xi) &= G(\xi) w(\xi) \\ &= c \frac{[\beta + (1-\beta)\cos(\xi h)][1 - \beta + \beta \cos(\xi h)]}{[1 - \beta + \beta \cos(\xi h)]^2 + \left[\frac{R}{2} \sin(\xi h), \right]^2} \end{aligned} \tag{95}$$

For the box method, (89) gives the interesting result

$$W(\omega) = c \cos^2 \left(\frac{\omega \Delta t}{2} \right), \tag{96}$$

which depends on Δt, but is independent of h. In the semi-discrete case ($R = 0$) this becomes

$$W = c, \tag{97}$$

which is equal to the exact value for solutions of (1).

The mathematics which describes energy flow also provides a link between x- and t-Fourier transforms: equating the energy flow (88) for a solution of p-type which is initially contained in $x < x_n$ with the expression (31a) for that energy gives the relation

$$|p(\xi, 0)| = |p_n(\omega)| G_p \tag{98}$$

8. THE BOUNDARY VALUE PROBLEM

We will, with the preceding mathematics, compare the responses of the algorithms under consideration when they are used to obtain a solution to the boundary value problem.

We consider the computing domain consisting of the half space

$$D \equiv x \geqslant 0, \tag{99}$$

and $x = 0$ is an upwind, closed boundary with

$$U(0, t) \text{ imposed.} \tag{100a}$$

It is assumed that the initial state is quiescent, i.e. that at some initial time we have

$$\{u_n(0)\} \equiv 0. \tag{100b}$$

Note that since the solution in D originates from the left, it may consist of rightgoing components only. ■

Accordingly, we have in response to (100a),

$$u_n^j = \int_{-\pi/\Delta t}^{\pi/\Delta t} \overline{u}_0(\omega)[\hat{E}_p(\omega)]^{(n)} e^{ij\omega\Delta t} \frac{d\omega}{2\pi} \tag{101}$$

(to be read [ ] to the power (n)), where $u_0(\omega)$ is the t-Fourier transform of $u(0,t)$ sampled at the discrete points $t^j = j\Delta t$:

$$\{u_0^j\} = \{U(0, j\Delta t)\}, \tag{102a}$$

$$\overline{u}_0(\omega) = \Delta t \sum_{j=-\infty}^{\infty} u_0^j e^{-ij\omega\Delta t}. \tag{102b}$$

The energy of u,

$$\mathscr{E}_\beta^j \equiv h \sum_{n>0} u_n^j \left[\frac{\beta}{2} u_{n-1}^j + (1-\beta) u_n^j + \frac{\beta}{2} u_{n+1}^j \right], \tag{103}$$

is of course not a constant, since energy is allowed to flow into D across the upwind boundary.

Assuming that $U(0,t)$ is in a Hilbert space (i.e. is of finite $\mathscr{L}_2$ norm), the total energy flowing into D will also be finite and may be expressed by

$$\begin{aligned} \mathscr{E}_\beta^\infty &= \lim_{j\to\infty} \mathscr{E}_\beta^i \\ &= \int_{-\omega_c}^{\omega_c} |\overline{u}_0(\omega)|^2 W(\omega) \frac{d\omega}{2\pi}, \end{aligned} \tag{104}$$

which becomes, in the semi-discrete case,

$$\begin{aligned} \mathscr{E}_\beta(\infty) &= \lim_{t\to\infty} \mathscr{E}_\beta(t) \\ &\int_{-\omega_c}^{\omega_c} |\hat{U}(0,\omega)|^2 W(\omega) \frac{d\omega}{2\pi}. \end{aligned} \tag{105}$$

Note the difference in the limits of integration between (101) and (104), (105): whereas Fourier components for $|\omega| \geqslant \omega_c$ are allowed in (101), only those corresponding to $|\omega| < \omega_c$ need be included in (104), (105), since those corresponding to higher frequencies do not carry energy, and their contribution to the integral is nil.

Although Fourier components of the solution corresponding to $|\omega| > \omega_c$ do not carry energy into D, they are nevertheless not identically zero. Their nature is analysed in the following section.

9. EVANESCENT SOLUTIONS

By the mathematics of the preceding sections, *when an upwind sinusoidal boundary condition is imposed with a frequency which exceeds the cut-off frequency, the solution in D cannot consist of a constant amplitude sinusoidal wave, nor can this solution carry energy away from the boundary.*

What exists in D in response to this boundary condition is an 'evanescent solution', which may be described with the expression (49) for $\hat{E}_p$ derived earlier.

With $|\omega| > \omega_c$ and for

$$u_0^j = e^{i\omega j\Delta t} \tag{106}$$

we find

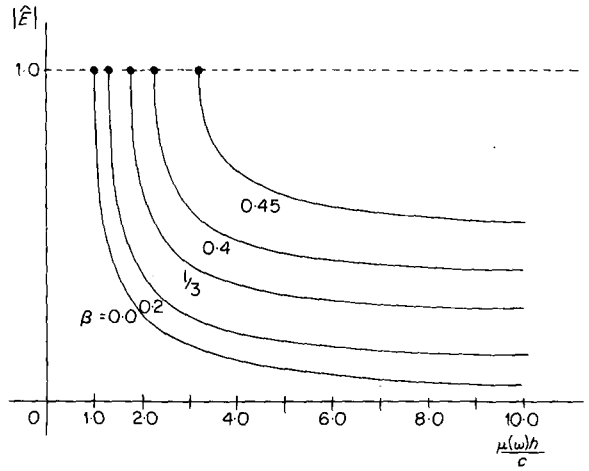

Figure 7. Amplitude decay per cell of the evanescent solutions as a function of frequency for $\beta = 0$, 0·2, 1/3, 0·4 and 0·45: —●— cut-off points

$$u_n^j = [\hat{E}_p(\omega)]^n e^{i\omega j\Delta t}, \tag{107}$$

where (Figure 7)

$$|\hat{E}_p(\omega)| = \left| \frac{-i\{(1-\beta)\bar{\mu} - \sqrt{[(1-2\beta)\bar{\mu}^2 - 1]}\}}{1 + i\beta\bar{\mu}} \right| < 1. \tag{108}$$

This solution consists of a sinusoidal function modulated by an envelope which decays exponentially with n, at a rate which increases with $|\omega| - \omega_c$. The asymptotic value of the amplitude decay per cell (measured by the absolute value of $\hat{E}$) is

$$\lim_{\omega \to \infty} |\hat{E}_p(\omega)| = \frac{1 - \beta - \sqrt{(1-2\beta)}}{\beta}, \tag{109}$$

which is zero in the finite difference case ($\beta = 0$), but remains finite in all the other cases.

The wavelength of the evanescent solutions is given by (Figure 8)

$$\lambda_e = \frac{2\pi h}{\frac{\pi}{2} + \arctan(\beta\mu(\omega))} = \frac{4h}{1 + \frac{2}{\pi}\arctan(\beta\mu(\omega))} \tag{110}$$

and is contained in

$$2h \leqslant \lambda_e \leqslant \lambda_c = \frac{4h}{1 + \frac{2}{\pi}\arctan\left(\frac{\beta}{\sqrt{(1-2\beta)}}\right)} \leqslant h. \tag{111}$$

With finite differences ($\beta = 0$) (110) becomes

$$\lambda_e = 4h, \tag{112}$$

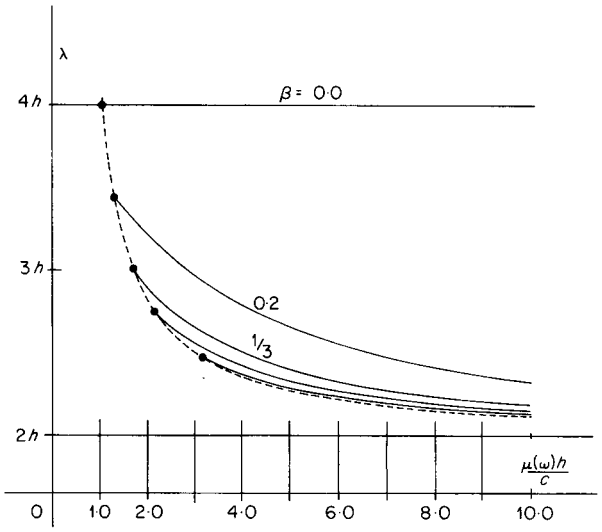

Figure 8. Wavelength of the evanescent solutions as a function of frequency for $\beta = 0, 0{\cdot}2, 1/3, 0{\cdot}4$ and $0{\cdot}45$: ——— cut-off curve; ●—— cut-off points

i.e. the evanescent solutions have in this case the constant wavelength $4h$ independently of ω. This interesting property was first described in Reference 11, and that it ceases for other values of β was noted by Foreman[15] in the context of a finite element/Galerkin approximation of the shallow water wave equations. Numerical illustrations are shown in Figure 9.

The case of the box method is again special: we have seen in section 4 that the cut-off frequency is then $\omega_c = \pi/\Delta t$, half the sampling frequency resulting from the time discretization step Δt: no components with a frequency $|\omega|$ beyond ω_c are present in $\{u_0^j\}$ after sampling of $U(0,t)$, and evanescent solutions simply do not exist. Moreover, for values of β which approach 1/2,

$$\lim_{\beta \to 1/2} |\hat{E}_p(\omega)| = 1, \quad |\omega| > \omega_c,$$
$$\lim_{\beta \to 1/2} \omega_c = \infty \tag{113}$$

(i.e. amplitude decay disappears as $\beta \to 1/2$).

If we consider the case of a boundary condition $\{u_0^j\}$ which is not a single frequency sinusoidal function, but is a general waveform of finite l_2 norm whose Fourier transform is contained, to within a remainder of negligible energy, in $|\omega| > \omega_c$, then (104) will give

$$\mathscr{E}_\beta^\infty = 0. \tag{114}$$

The solution in D is however not identically zero: it is still expressed by (101). But although energy flows into D during some of the time, it eventually returns entirely to the left across the boundary.

Other than in the case of the boundary value problem described here, evanescent solutions also appear in the cases of internal reflection that will be examined in sections 11 and 15.

10. STEP RESPONSES

There are significant differences in the manners in which the different algorithms considered

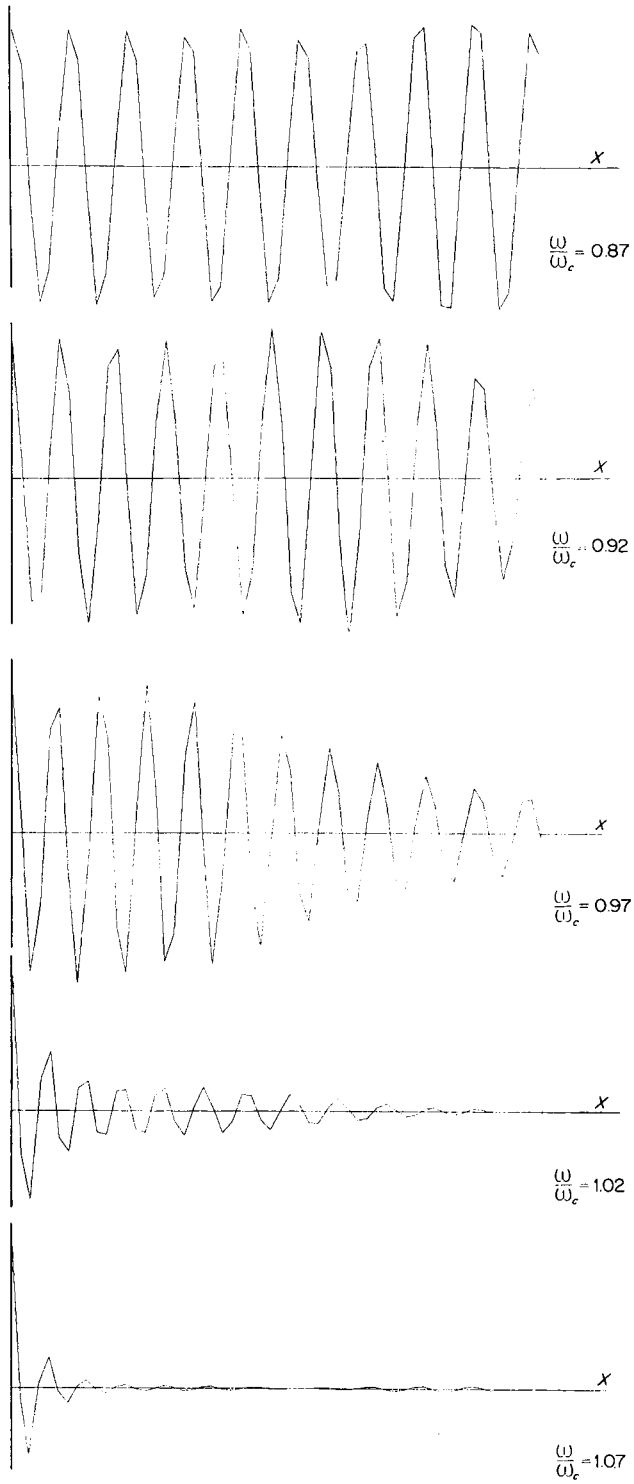

Figure 9. Response at $t = 150$ to a sinusoidal boundary condition beginning at $t = 0$ at the upwind boundary. $R = 0{\cdot}5$; $\omega_c = 0{\cdot}98$; $\beta = 0$. Note the sharpness with which the solutions pass from constant-amplitude to evanescent when ω passes through ω_c. Note also that (to the accuracy afforded by visual observation) $\lambda = 4h$ in all cases where $\omega \geqslant \omega_c$

respond to a step change in the imposed value at an upwind boundary. As will be shown below, those step responses may vary significantly with both β and R.

We consider the initial/boundary value problem

$$D \equiv x \in [0, \infty); \quad u_n^0 = 0; \quad n = 1, 2, 3, \ldots, \tag{115}$$

with

$$u_0^j = 1; \quad j = 0, 1, 2, \ldots \tag{116}$$

The discrete t-Fourier transform of (107) is

$$\bar{u}_0(\omega) = \frac{\Delta t}{2i \sin(\omega \Delta t/2)} e^{-i\omega \Delta t/2}. \tag{117}$$

What is important in this expression is that it contains a significant amount of energy in the higher frequencies, where phase and group velocity errors are significant.

Step responses for $\beta = 0$ (the finite differences case), $\beta = 1/3$ (the finite elements case) and $\beta = 1/2$ (the box scheme) are illustrated in Figures 10(a)–10(c) together with an interpretation of the observed difference in the light of the wave propagation properties of these algorithms derived earlier in this paper.

It should be mentioned that several of those step responses may be expressed in closed analytic form.[4]

PART II: REFLECTION PHENOMENA

11. WAVE REFLECTION I: MESH REFINEMENT

It is in the investigation of parasitic phenomena associated with boundaries and irregular grids that the Fourier analysis/wave propagation viewpoint takes its full power. Representative contributions to this question include those of Browning, Kreiss and Oliger,[12] Chu and Sereny,[13] Engquist and Majda,[14] Vichnevetsky,[21,36] Halpern,[16] Trefethen,[18,19] Foreman[15] and Wagatha.[25]

The mesh refinement problem serves as a convenient device for the introduction of the relevant concepts and mathematics entering in the analysis of spurious reflection (also called scattering): consider two piecewise uniform discretizations of the x axis which interface at $x = 0$ (Figure 11):

$$\begin{aligned} x_n &= nh_L, \quad \text{when} \quad n < 0, \\ x_n &= nh_R, \quad \text{when} \quad n > 0. \end{aligned} \tag{118}$$

A natural way to extend (12) is then

$$M\left[\frac{\beta}{2} u_{n-1}^j + (1-\beta) u_n^j + \frac{\beta}{2} u_{n+1}^j\right] = -c\left(\frac{u_{n+1}^j - u_{n-1}^j}{2h_L}\right) \tag{119a}$$

when $n < 0$,

$$M\left[\frac{\beta}{2} u_{n-1}^j + (1-\beta) u_n^j + \frac{\beta}{2} u_{n+1}^j\right] = -c\left(\frac{u_{n+1}^j - u_{n-1}^j}{2h_R}\right) \tag{119b}$$

when $n > 0$, and

$$M\left[\frac{\beta h_L}{h_L + h_R} u_{-1}^j + (1-\beta) u_0^j + \frac{\beta h_R}{h_L + h_R} u_1^j\right] = -c\left(\frac{u_1 - u_{-1}}{h_L + h_R}\right) \tag{119c}$$

when $n = 0$.

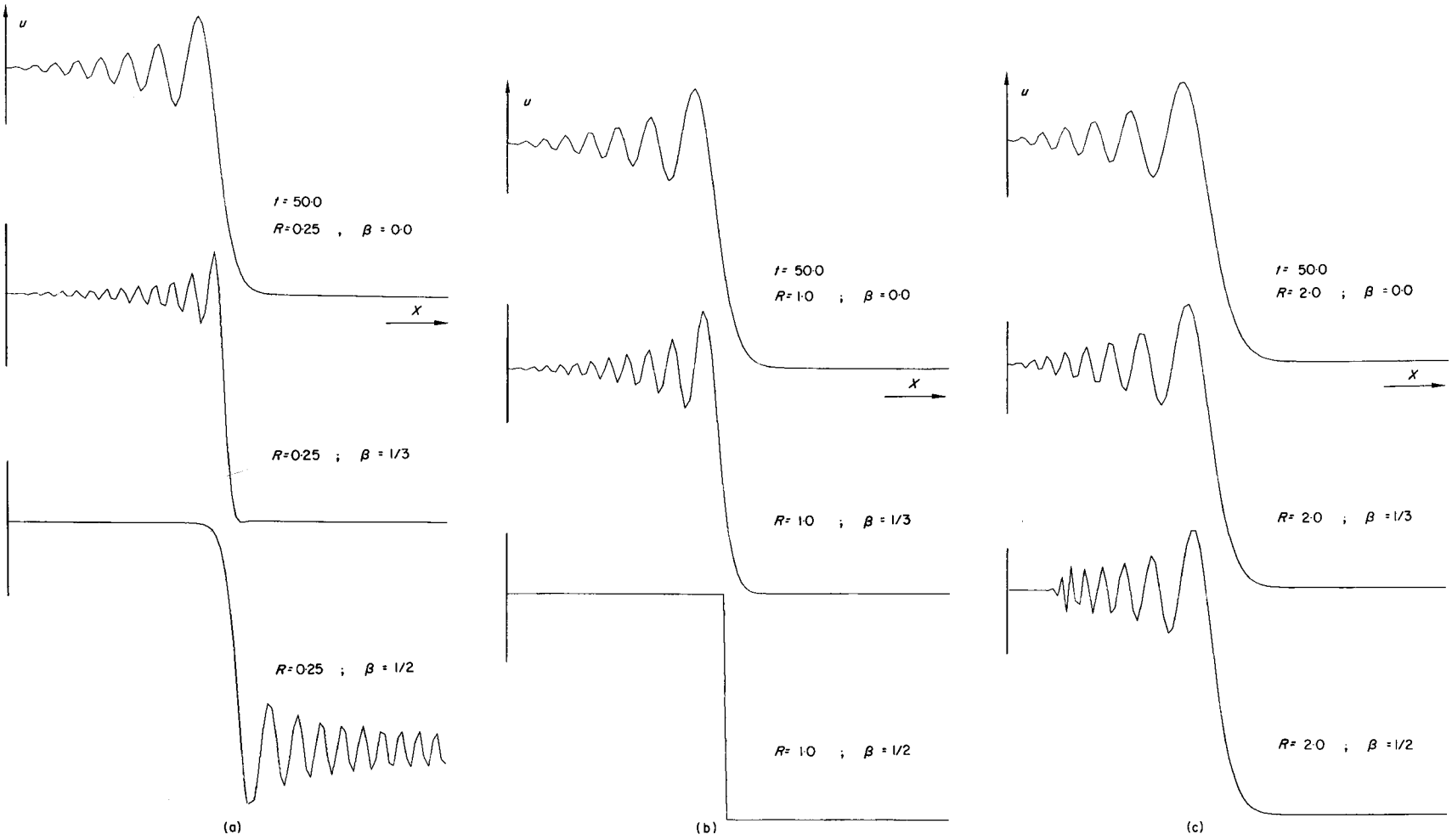

Figure 10. $u(x, 50)$ in response to a unit step applied in $t = 0$ at the boundary $x = 0$. The differences observed between the different cases can be entirely explained by phase velocity considerations. (a) $R = 0{\cdot}25$: phase velocities are close to those predicted by the semi-discrete model (see also Figure 1). The box method has the interesting property of having phase velocities larger than c. (b) $R = 1$: the box method becomes exact. (c) $R = 2$: the phase velocities are approaching those resulting from the time stepping approximation alone, which is the same in all three cases

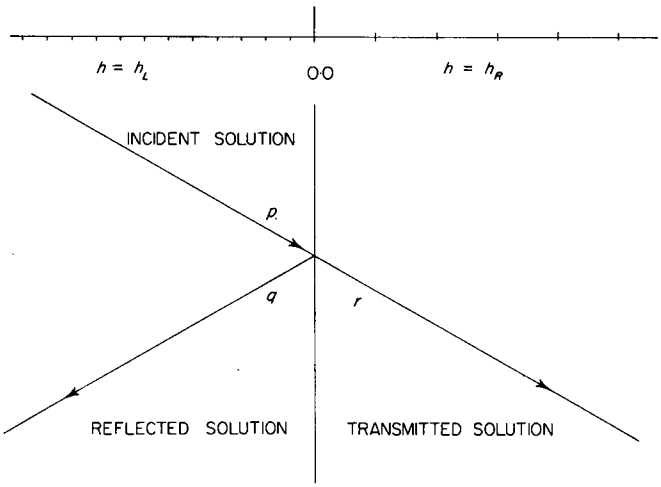

Figure 11. Mesh refinement

The equation (119c), which applies at the interface point, is obtained when the weighted residual procedure (5)–(7) is extended to allow for a non-constant h by letting

$$g_0(x) = \begin{cases} 1, & \text{in } x \in [-2\beta h_L, 2\beta h_R] \\ 0, & \text{elsewhere.} \end{cases} \tag{120}$$

It may be verified, by the same construction as that of section 3, that the corresponding energy, defined on an irregular grid as

$$\mathscr{E}_\beta = \sum_{n=-\infty}^{\infty} u_n \left[\frac{\beta}{2} h_n u_{n-1} + (1-\beta)\left(\frac{h_n + h_{n+1}}{2}\right) u_n + \frac{\beta}{2} h_{n+1} u_{n+1} \right], h_n \equiv x_n - x_{n-1}, \tag{121}$$

is again an invariant with respect to time when $\{u_n^j\}$ is a solution of (119). As in the regular mesh case (h = constant), this implies stability for the Cauchy problem in the $\mathscr{E}_\beta$ norm. It should also be noted that no such invariance principle applies to the l_2 energy of solutions of the Cauchy problem for (119).

When a rightgoing solution arrives from the left, then a process of reflection or scattering takes place at the interface. The appropriate tool to be used for the analysis of this is that given by t-Fourier transforms, not x-Fourier transforms. The reason why this is so is that *the frequency ω (the dual variable of t-Fourier transforms) of a sinusoidal wave is preserved during reflection whereas its wave number ξ is not.* ■

Consider thus in $x < 0$ a solution of p type which arrives at the interface (Figure 11). Let $p_0(\omega)$ be the Fourier transform of the incident solution arriving at $x = 0$, $q_0(\omega)$ be the Fourier transform of the reflected solution at the same point and $r_0(\omega)$ be the Fourier transform of the resulting rightgoing solution in $x > 0$.

The amount of reflection is expressed in Fourier space by the amplitude reflection ratio

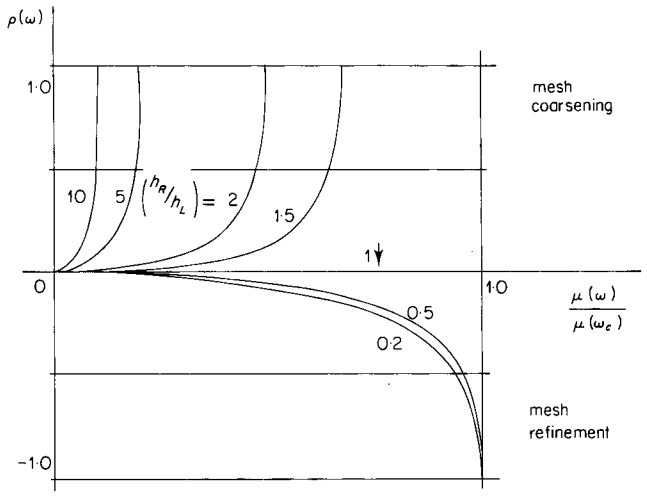

Figure 12. Amplitude reflection ratio in mesh refinement. With the frequency normalization used on the horizontal axis, this Figure is the same for all values of β

$$\frac{\bar{q}_0(\omega)}{\bar{p}_0(\omega)} \equiv \rho(\omega) = \frac{\sqrt{\left[1-(1-2\beta)\left(\frac{\mu h_L}{c}\right)^2\right]} - \sqrt{\left[1-(1-2\beta)\left(\frac{\mu h_R}{c}\right)^2\right]}}{\sqrt{\left[1-(1-2\beta)\left(\frac{\mu h_L}{c}\right)^2\right]} + \sqrt{\left[1-(1-2\beta)\left(\frac{\mu h_R}{c}\right)^2\right]}}$$

$$= \frac{W_L(\omega) - W_R(\omega)}{W_L(\omega) + W_R(\omega)}, \tag{122}$$

(Figure 12): which is obtained by Fourier transforming equation (119c) and eliminating values of the solution in $n = 1$ and $n = -1$ by use of (49) and (50).[21]

If we were interested in suppressing reflection for a specific frequency ω_0, this could be achieved for instance by choosing different values for β on the left and right half axes, so as to equate $W_L(\omega_0)$ and $W_R(\omega_0)$. Although possibly of little interest in numerical analysis, this is closely related to the process of 'impedance matching' well known in the field of communications engineering.

During reflection, the wave numbers of the incident and reflected waves are related by the fact that they correspond to the same value of ω in the dispersion relation (see Figure 13). We may note that this relation is independent of Δt: indeed, the relation between the two roots ξ_p and ξ_q, which are obtained when (22) is solved for ξ with ω given, is independent of Δt. This property is an expression of a more general invariance principle to which we shall return in section 13.

In the particular case of well resolved incident solutions arriving at the interface (these are solutions corresponding to wave numbers near $|\xi h_L| = 0$) the reflected solutions have wave numbers near $|\xi h_L| = \pi$, or wavelengths near $\lambda = 2h_L$, which results in their typical saw-toothed appearance (this holds for all values of β): spurious solutions of this kind are illustrated in Figure 14.

We may use (122) to measure the reflection of energy; the corresponding reflection ratio is simply the square of the amplitude reflection ratio:

$$\frac{\phi_\beta^R(\omega)}{\phi_\beta^I(\omega)} = \frac{|q_0(\omega)|^2 W_L(\omega)}{|p_0(\omega)|^2 W_L(\omega)} = |\rho(\omega)|^2, \tag{123}$$

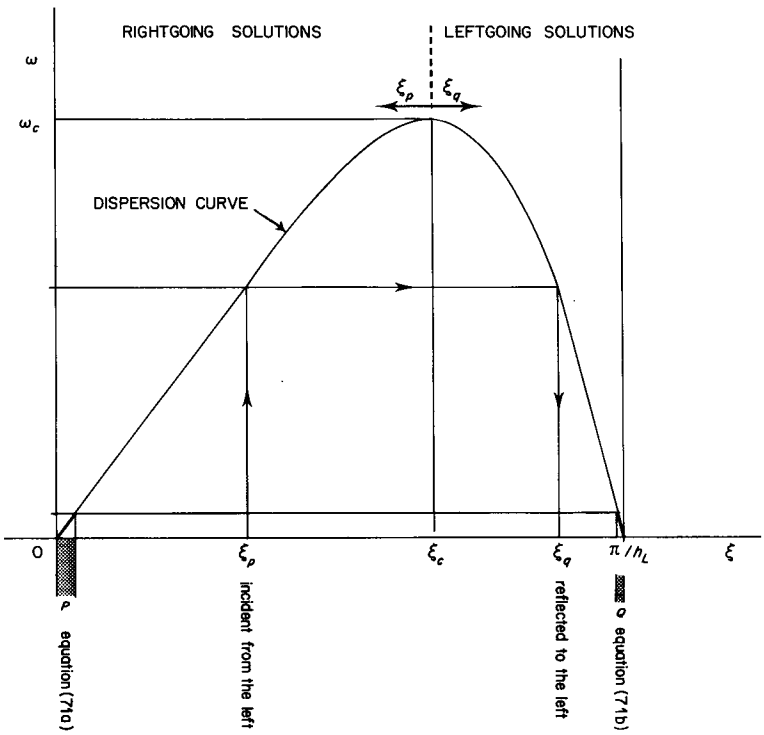

Figure 13. During reflection, the wave numbers of the incident and reflected solutions are related by the fact that they belong to the same frequency ω (which is an invariant) on the dispersion curve. Well resolved solutions arriving from the left correspond to $|\xi_p h_L| \to 0$, and the resulting reflected solutions thus correspond to $|\xi_q h_L| \to \pi$. When R is finite, then these 2 types of solutions are described by equations (71a) and (71b), respectively

where

$$\phi_\beta^I(\omega) = |\overline{p_0}(\omega)|^2 W_L(\omega) \tag{124a}$$

and

$$\phi_\beta^R(\omega) = |\overline{q_0}(\omega)|^2 W_L(\omega) \tag{124b}$$

are the spectral distributions of the flows of incident and reflected energy at the interface point.

From this we obtain the expression of the reflected energy (in $x < 0$):

$$\mathscr{E}_\beta^R = \int_{-\omega_c}^{\omega_c} |p_0(\omega)\rho(\omega)|^2 W_L(\omega) \frac{d\omega}{2\pi} \tag{125}$$

and that of the transmitted energy (in $x > 0$):

$$\mathscr{E}_\beta^T = \int_{-\omega_c}^{\omega_c} |\overline{p_0}(\omega)(1 + \rho(\omega))|^2 W_R(\omega) \frac{d\omega}{2\pi}. \tag{126}$$

One may verify with (122) that the following identity holds:

$$W_L = \rho^2 W_L + (1 + \rho)^2 W_R. \tag{127}$$

Together with the above, this results in a simple expression of the conservation of energy flows across the mesh refinement interface:

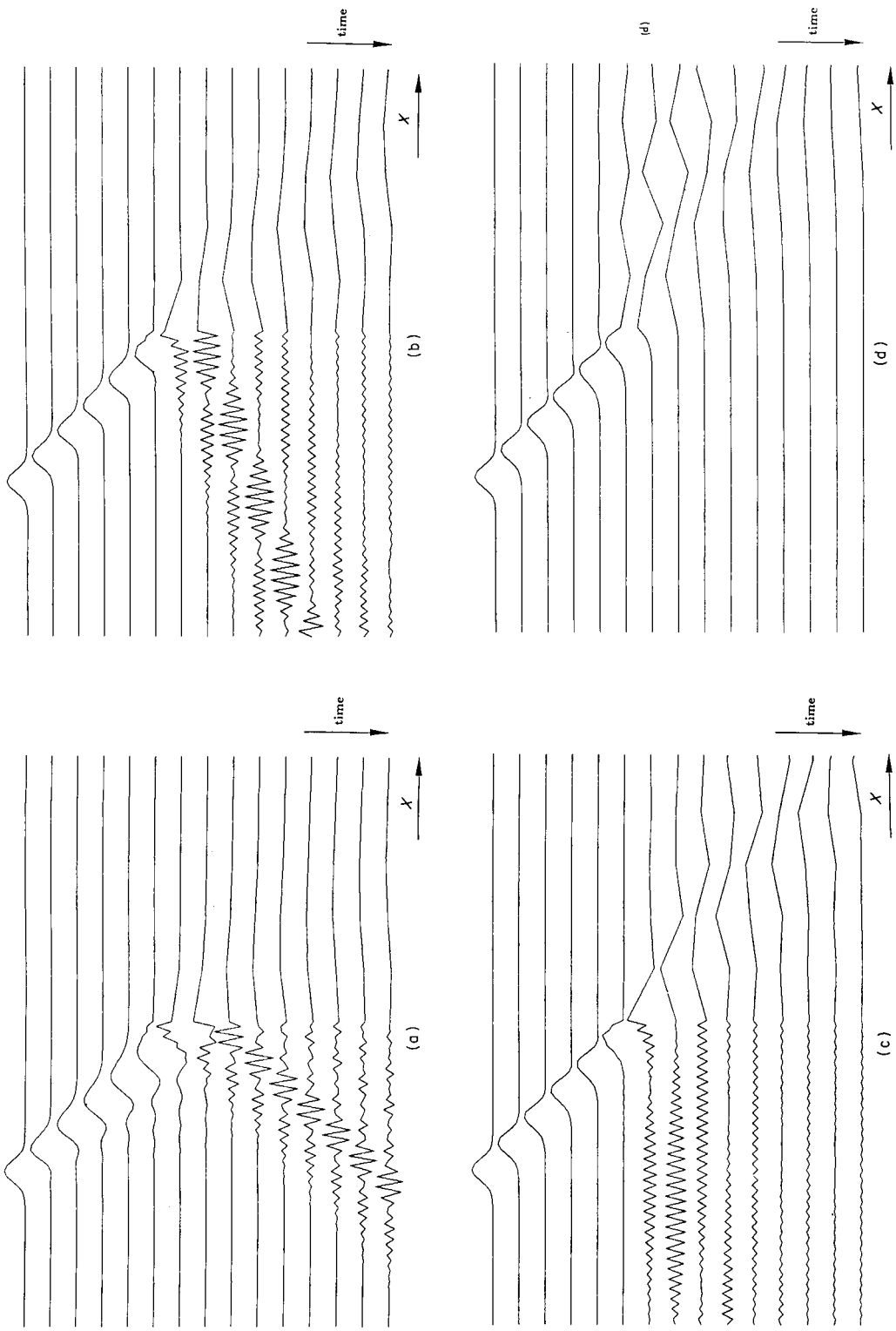

Figure 14. Reflection of a smooth solution at a mesh coarsening interface. The initial function is a Gaussian with $\sigma = 2$, $h_L = 1$, $h_R = 10$; $\Delta t = 0{\cdot}25$. Note that there is no reflection in the box case (d). The absorbing scheme (140) is used at the upwind boundary to the left, and the computing domain extends well beyond the Figure to the right: (a) $\beta = 0$; (b) $\beta = 1/3$; (c) $\beta = 0{\cdot}45$; (d) $\beta = 0{\cdot}5$

$$\mathscr{E}_\beta^{\mathrm{I}} = \mathscr{E}_\beta^{\mathrm{R}} + \mathscr{E}_\beta^{\mathrm{T}} \tag{128}$$

where $\mathscr{E}_\beta^{\mathrm{I}}$ is the incident energy contained in p_0. It has been noted earlier that, by contrast, no conservation of the l_2 energy applies during reflection.

In the particular case of the box method we find

$$\rho_{\beta=1/2}(\omega) \equiv 0. \tag{129}$$

There is no reflection at the mesh refinement interface. An illustration of this is given in Figure 14(d).

A remark concerning those wavelengths coming from the left for which there is total reflection: these occur in mesh coarsening for frequencies which are in the band

$$\omega_{\mathrm{c,R}} = \frac{c}{h_{\mathrm{R}}\sqrt{(1-2\beta)}} < |\omega| < \omega_{\mathrm{c,L}} = \frac{c}{h_{\mathrm{L}}\sqrt{(1-2\beta)}} \tag{130}$$

The amplitude reflection ratio has then an absolute value of one, and all the incident energy ends up in a leftgoing reflected solution. The reflection process is however not strictly localized in $x = 0$. During reflection, an evanescent solution appears in $x > 0$. Some of the incident energy goes into that evanescent solution and returns to the left later on when the reflection process is completed. The coarse mesh in $x > 0$ acts as soft elastic wall for wave groups of frequency in (130), which behave correspondingly as solid bouncing particles. If the right hand boundary were at a finite distance from the interface (instead of being at what amounts in practice to infinity), then some of the energy contained in the tail of the evanescent solution would reach that boundary and escape to the right and not return to the left. This is analogous to the process of 'tunnelling' in quantum mechanics:[37] in the latter case, evanescent solutions of Schrödinger's equation appear in $x > 0$.

We also note that the situation just analysed is similar, in the semi-discrete case, to certain well-known results concerning propagation properties of mechanical structures and electrical networks. Compare for instance Figure 11 with Figure 14.2 of Reference 30 and equation (122) with equation 23·17 of the same reference. The fact that relations such as (122) continue to apply strictly when time is discretized as well is however a new result: only inside numerical simulations does discrete-space–discrete-time propagation exist.

12. WAVE REFLECTION II: DOWNWIND BOUNDARIES

If we let $h_{\mathrm{L}} = h$ and $h_{\mathrm{R}} \to 0$, in (119), then (119a) becomes identical to (12) and (119c) becomes

$$M[\beta u^i_{-1} + (1-\beta)u^j_0] = -c\left(\frac{u^j_0 - u^j_{-1}}{h}\right), \tag{131}$$

which is the natural form of a boundary scheme to be used when the computational domain is the half space to the left of $x = 0$, and $x = 0$ is an open, downwind boundary.

Letting $h_{\mathrm{R}} \to 0$ in (122) gives the corresponding amplitude reflection ratio (Figure 15):

$$\begin{aligned}\rho(\omega) &= \frac{\sqrt{[1-(\mu(\omega)/\mu(\omega_{\mathrm{c}}))^2]} - 1}{\sqrt{[1+(\mu(\omega)/\mu(\omega_{\mathrm{c}}))^2]} + 1} \\ &= \frac{W(\omega) - c\cos^2\left(\dfrac{\omega\Delta t}{2}\right)}{W(\omega) + c\cos^2\left(\dfrac{\omega\Delta t}{2}\right)},\end{aligned} \tag{132}$$

and the energy reflected at the boundary is, as in the preceding case, expressed by (125), with $\rho(\omega)$ given by the above.

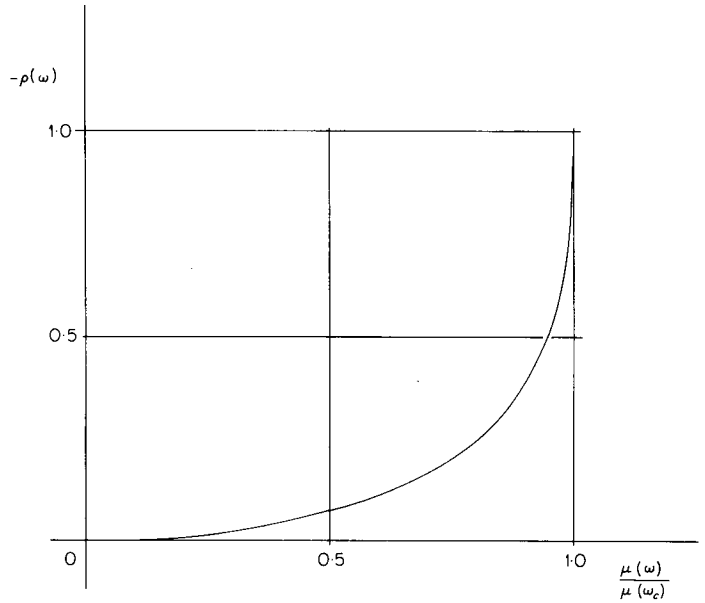

Figure 15. Amplitude reflection ratio for the natural boundary scheme (131). As for Figure 12, this Figure is the same for all values of β

If we pursue the analysis of the preceding section, we may apply the energy conservation relation (128) to the present case by considering that the energy flowing outside D is still given by (126), with

$$W_R(\omega) = W_{h=0} = c\cos^2\left(\frac{\omega\Delta t}{2}\right) \tag{133}$$

(compare with (96)).

It is to be noted that, as in the case of mesh refinement, the box method has the interesting property that it creates no reflection at the downwind boundary.

The analytical description of amplitude reflection at mesh interfaces and boundaries (equations (122) and (132)) has been expressed by using only the characteristic admittance $W(\omega)$ to describe the properties of the corresponding computing subdomains. As was shown in section 7, $W(\omega)$ appears when wave analysis is considered from the viewpoint of energy propagation. Together with relations of the kind expressed by (128), this emphasizes the role played by energy concepts in the mathematical description of (parasitic) reflection at mesh refinement interfaces and at boundaries.

It may be useful to summarize this and previous remarks as follows. *The process of wave reflection at boundaries and mesh refinement interfaces has two invariants: the frequency* ω and the energy $\mathscr{E}_\beta$ ■

Implicit in the above is the fact that the natural way to write boundary and interface equations is being used (namely (119) and (131), which are consistent with (12)).

Note, however, that this natural way of treating interfaces and boundaries is not necessarily the best. This will be illustrated with the following example in which the box algorithm, i.e. (131) with $\beta = 1/2$:

$$M\left(\frac{u^j_{-1} + u^j_0}{2}\right) = -c\left(\frac{u^j_0 - u^j_{-1}}{h}\right), \tag{134}$$

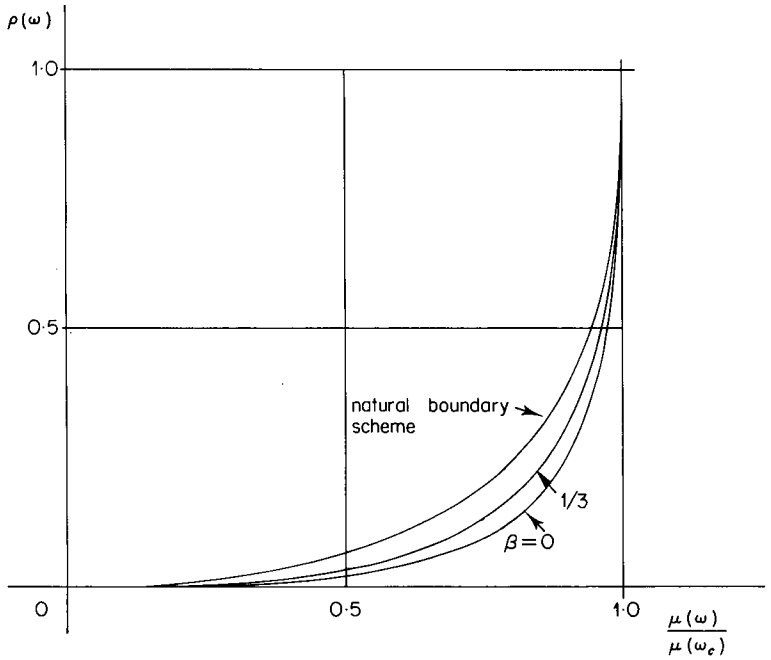

Figure 16. Comparison of the amplitude reflection ratio generated by the box scheme used at the downwind boundary of a computing domain in which the approximation uses another value for β (bottom curves) with that generated by the natural boundary scheme (131) (top curve)

is used at the downwind boundary of a computing domain where (12) applies with another value for β. The general expression of the corresponding amplitude reflection ratio is

$$\rho_B \equiv \frac{q_0(\omega)}{p_0(\omega)} = -\frac{\left(1+\frac{i\bar{\mu}}{2}\right)-\hat{E}_p^{-1}\left(1-\frac{i\bar{\mu}}{2}\right)}{\left(1+\frac{i\bar{\mu}}{2}\right)-\hat{E}_q^{-1}\left(1-\frac{i\bar{\mu}}{2}\right)} \tag{135}$$

where $\hat{E}_p(\omega)$ and $\hat{E}_q(\omega)$ (equations (49) and (50)) describe the wave propagation properties in D. It may be verified that this expression converges to zero as $O(\omega^3 h^3)$. By contrast, the amplitude reflection ratio (132) corresponding to the natural treatment of the boundary converges to zero only as $O(\omega^2 h^2)$. A graphical comparison is given in Figure 16.

This superior property of the box algorithm used at the boundary with some other algorithm used in D has not escaped the attention of workers in the field. For instance, mention of this may be found in References 13 and 15, both having to do with numerical approximations of the shallow water wave equations.

13. AN INVARIANCE PRINCIPLE

We have made earlier reference to an important independence (or invariance) principle which applies to the class of reflection phenomena that have been examined. One of its expressions may be stated in the form of a theorem (from Reference 38, where a formal proof may be found).

Consider, for the mesh refinement problem of section 11 or the downwind boundary problem of section 12, an initial function $\{u_n^0\}$ which is imposed to the left of the reflection point. The

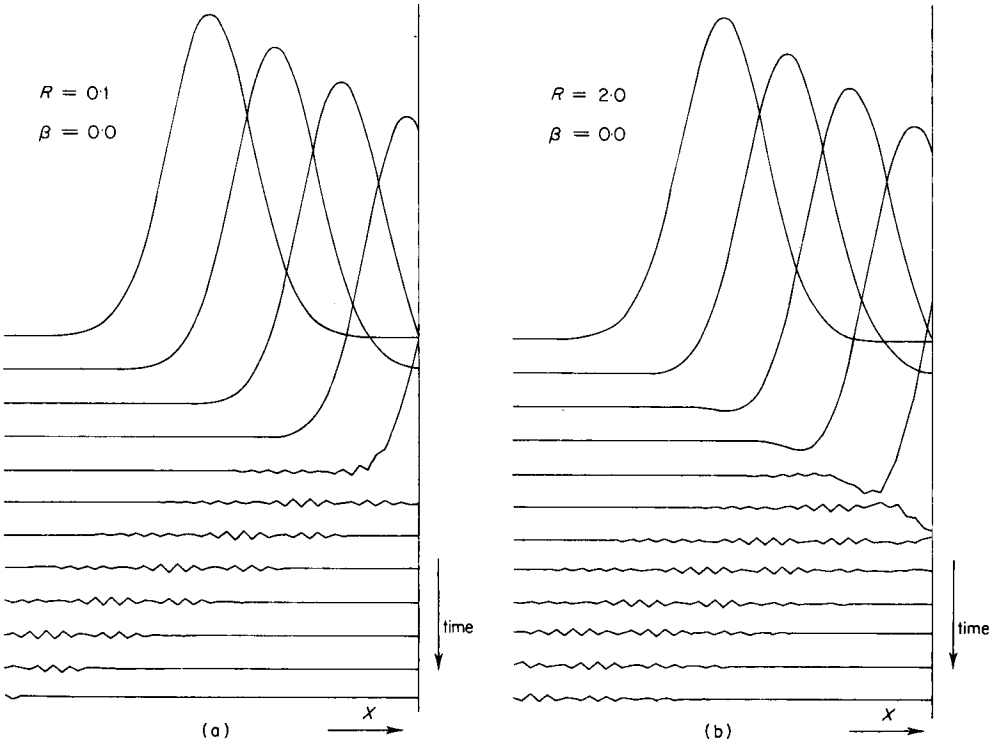

Figure 17. Comparison of two solutions with different values of Δt: $U(x,0) = e^{-1/2[(x-x_0)/\sigma]^2}$; $\sigma = 10$; $h = 1$ in both cases

rightgoing portion of this initial function will be partially reflected at x_0 as described by the expression (125) of the reflected energy. Then

Theorem. The energy $\mathscr{E}_\beta^R$ reflected at x_0 is invariant under time discretization, i.e. is independent of the value of Δt used in the time stepping algorithm. It is strictly equal to the energy reflected in the semi-discrete case (when $M = d/dt$).

Although the nature of the numerical solution may be significantly different when the value of Δt is changed, what this theorem states is that, somewhat unexpectedly, this difference leaves the reflected energy invariant, as long as the initial data $\{u_n^0\}$ are left unchanged.

Given in Figure 17 and 18 are the results of a numerical experiment which verifies this theorem. A more general (if less precise) statement of this principle is as follows: *In those numerical schemes which are obtained (as in this paper) by applying to a spatial semi-discretization of the equations the same conservative and stable time discretization algorithm consistently everywhere (= method of lines), and in those cases where initial data only are specified, the total energy transmitted or reflected at any given point of the computing domain depends on the space discretization alone.* ■

Instances of the application of this principle are noted elsewhere in this paper (cf. sections 11 and 15).

This invariance principle has interesting implications, namely

(i) As long as parasitic solutions are measured in the appropriate energy norm, the analysis of many spurious reflection phenomena may be analysed in the semi-discrete case—which is simpler than the fully discrete case.

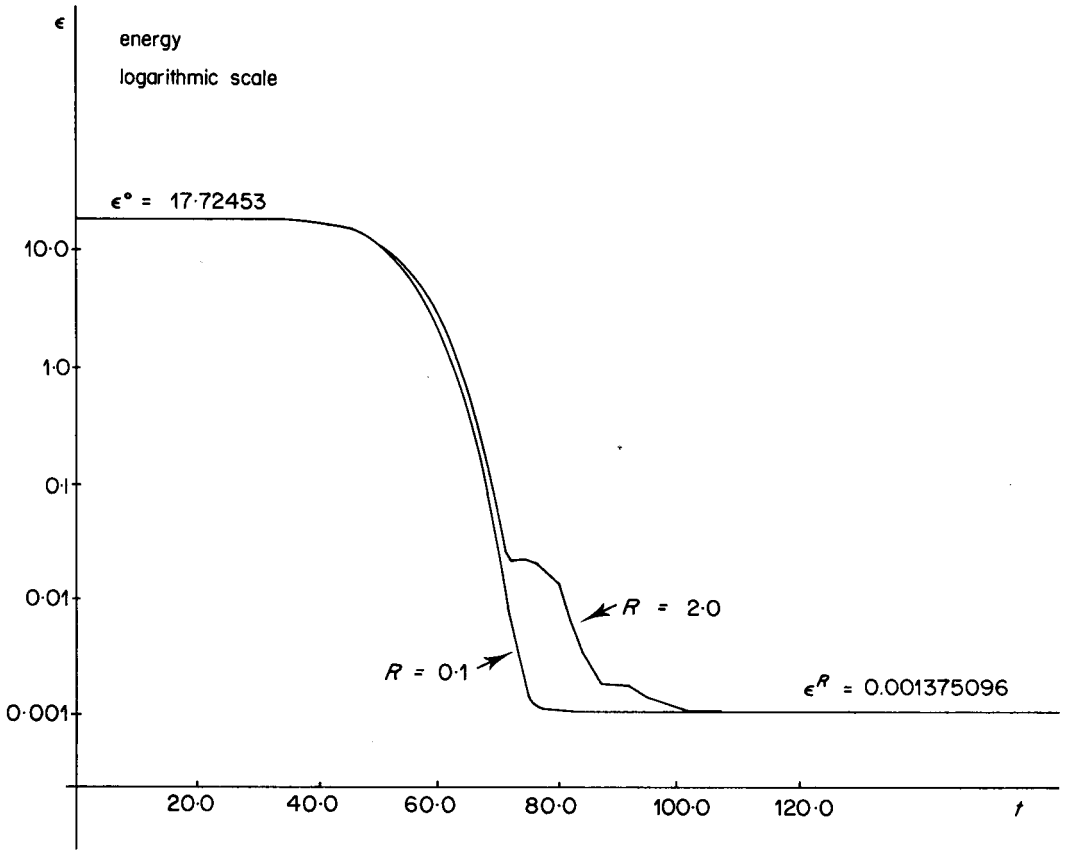

Figure 18. Energy versus time for the numerical experiments shown in Figures 17(a) and 17(b). Although the time histories are different, the total energies reflected are the same for the two cases. Values of $\mathscr{E}^R$ measured at $t = 120$ differ only in the last significant digit (as explained by differences in round-off error)

(ii) Corresponding absorbing boundary and interface schemes may likewise be synthesized for the semi-discrete equations: their energy absorbing properties will remain invariant under time-discretization.[23,24]

14. WAVE REFLECTION III: UPWIND BOUNDARIES

Parasitic reflection also takes place at upwind boundaries. To illustrate this, we return to the domain (99) and consider the case where a solution of q type arrives from the right at $x = 0$, where the condition

$$U(0, t) = 0 \tag{136}$$

applies. When this condition is translated into

$$u_0^j = U(0, t^j) = 0, \tag{137}$$

then this results in

$$\overline{u}_0(\omega) = \overline{p}_0(\omega) + \overline{q}_0(\omega) = 0, \tag{138}$$

giving the amplitude reflection ratio

$$\rho(\omega) \equiv \frac{\overline{p_0}(\omega)}{\overline{q_0}(\omega)} = -1. \tag{139}$$

That $|\rho(\omega)| = 1$ implies total reflection of the energy at the boundary. What may be bothersome in this process is that whereas the incident leftgoing solution is clearly spurious, with the typical saw-toothed, short wavelength appearance, the reflected solution, which is of p type, consists of long wavelength components which cannot be distinguished from the consistent approximation of a true solution (see, for instance, Figure 6 in Reference 22).

The modified treatment of the upwind boundary:[24]

$$u_0^j = 2U(0, t^j) - u_1^j = -u_1^j \tag{140}$$

used to replace (137) has the property of absorbing spurious solutions instead of reflecting them. A geometrical interpretation of this formula is that it consists of imposing $U(0, t)$ at the mid-point $(x_0 + x_1)/2$, instead of imposing it at the mesh point x_0. (An early description of a similar scheme may be found in Reference 39.)

The corresponding amplitude reflection ratio is easily derived (with (66)):

$$\rho_a = -\frac{1 + e^{i\xi_q h}}{1 + e^{i\xi_p h}}. \tag{141}$$

As may be verified, there is perfect absorption of solutions of wavelength $2h$:

$$\rho_a(\xi_q h = \pi) = 0. \tag{142}$$

A detailed analysis of other properties of this scheme is given in Reference 24 for the finite difference case.

15. WAVE REFLECTION IV: INTERNAL REFLECTION IN NON-UNIFORM GRIDS

A different type of reflection may occur at interior points of a non-uniform, continuously variable grid. There are applications where such grids play an important role. One of these (which leads to large computer codes) is in the calculation of pressures and flows around aerofoils by numerical integration of the Euler equations of gas dynamics.[40–42]

Published results on numerical wave propagation in irregular grids for hyperbolic equations are relatively few. Early mention of this problem may be found in References 43 and 44. One of the first detailed theoretical analyses is that of Giles and Thompkins,[45,49] who used the so called 'asymptotic' method of standard wave propagation theory to derive some of the basic relations that apply to numerical schemes. Propagation in an irregular grid is also examined briefly by Trefethen[18,19] and by Chin and Hedstrom[46] with special attention to the problem of scattering. An analysis of this problem with the mathematics of sinusoidal wave propagation in inhomogeneous media may be found in Reference 42.

The expression which generalizes (12) to the case of a one-dimensional irregular grid is (compare with (119c))

$$M\left(\frac{\beta h_n}{h_n + h_{n+1}} u_{n-1}^j + (1-\beta) u_n^j + \frac{\beta h_{n+1}}{h_n + h_{n+1}} u_{n+1}^j\right) = -c\left(\frac{u_{n+1}^j - u_{n-1}^j}{h_n + h_{n+1}}\right), \tag{143}$$

where $h_n = x_n - x_{n-1}$ is the local mesh size. It may be verified, by using again the same procedure as that used in section 3, that the energy $\mathscr{E}_\beta$ expressed by (121) is strictly invariant with respect to time when $\{u_n^j\}$ is a solution of the Cauchy problem for (143).

When h_n varies slowly with respect to x (or n), the wave propagation in the corresponding linear, dispersive, non-homogeneous medium is characterized by the following properties:[42,47]

(i) Wave packets of frequency ω and wave number ξ are propagated locally as if the mesh were uniform.

(ii) During the motion of such wave packets, the frequency ω remains constant, and satisfaction of the dispersion relation (22) with h variable results in an x dependence of the wave number ξ.

(iii) The group velocity is given by (63) with h dependent on x and is thus also variable.

(iv) Restricting the discussion to the case $\beta \leqslant 1/3$: rightgoing wave packets in an expanding mesh ($dh/dx > 0$) have a continuously decreasing group velocity. They may, instead of leaving the computing domain through the downwind boundary, reach an internal point where the group velocity vanishes. This occurs when

$$h = h_r = \left| \frac{c}{\mu(\omega)} \frac{1}{\sqrt{(1-2\beta)}} \right|. \tag{144}$$

The wave packet is then reflected from rightgoing to leftgoing.

(v) The same is true for leftgoing wave packets in a contracting mesh ($dh/dx < 0$) which may be reflected internally from leftgoing to rightgoing.

A different expression of the principle of independence of section 13 applies here: the location of the internal reflection points defined by (144) is independent of time discretization. Indeed, a wave packet may be assumed to have been imposed as initial data with given ξ_0 and h_0. This defines $\mu(\omega)$ (an invariant of the wave packet) by the right hand side of (22). Inserting this value of μ in (144) leaves no relationship of h_r either to Δt, or even to the specific form assumed by $\mu(\omega)$.

It may be the case that the same wave packet experiences successively both types of internal reflection. An example of this is illustrated in Figure 19 (similar results are given by Giles and Thompkins[45,49]). When this kind of multiple internal reflection occurs in practice, then this may result in numerical simulations which cannot reach a steady state, irrespectively of the fact that genuine solutions do reach a steady state in a finite time. This takes place, for example, in certain large exterior aerodynamic calculations.[40,41] A common remedy for this kind of ailment consists of using artificial dissipation.

The analogy with quantum mechanics which was noted earlier applies here also: the propagation of a wave packet in a non-uniform grid is similar to the motion of an elementary particle in a space dependent potential field. The mathematics of the two are almost identical, and the trajectory of the wave packet illustrated in Figure 19 is the same as that of a particle in a smooth potential well.[37]

The analogy goes further: the continuous decrease in group velocity experienced by the wave group as a whole as in Figure 19 follows the continuous (and slow) variation in the mesh size. But if mesh size variations were abrupt instead of continuous, then scattering world occur at the interface and part of the wave group would be reflected in the opposite direction. Examples of this have been illustrated in section 11, and a further example is given in Figure 20. The physical analogue of this is in the process of scattering which occurs when a beam of particles passes across a step change in the potential, as described by the mathematics of quantum mechanics (see e.g. Reference 48, pp. 36, 37).

16. LEFTGOING SOLUTIONS OF THE BOX METHOD

The analysis has shown that the box method is a singular point in the family of algorithms

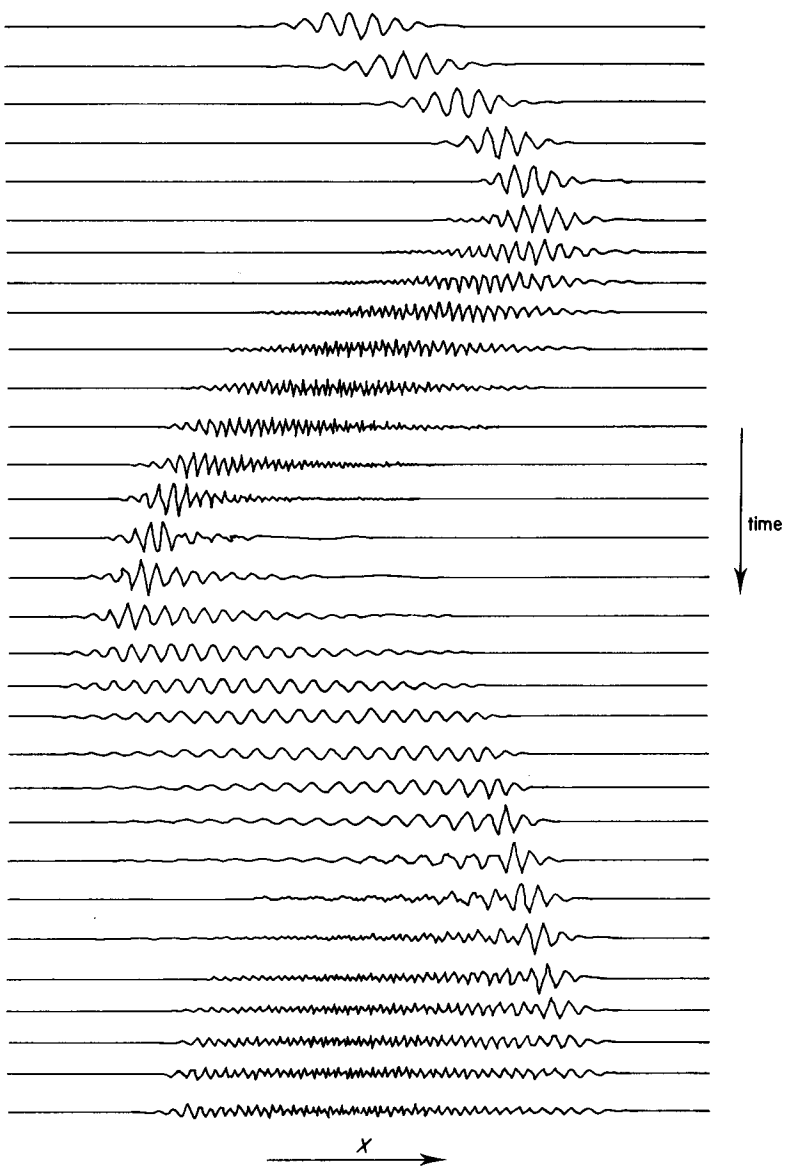

Figure 19. Multiple reflection of a wave packet in a 'grid well'. The mesh size is $h = 1$ at the centre and increases geometrically by 1 per cent per node symmetrically in both directions to reach $h = 3{\cdot}3$ at the boundaries ($\beta = 0, \Delta t = 0{\cdot}25$)

represented by (12). Instead of displaying rightgoing and leftgoing solutions in response to appropriate initial conditions, only rightgoing solutions are obtained. And likewise, no reflection from rightgoing to leftgoing occurs when mesh interfaces and boundaries are handled consistently.

But the box method may be considered as the limit case

$$\beta = \lim_{\delta \to 0} \left(\frac{1}{2} - \delta \right). \tag{145}$$

Accordingly, solutions of q type must exist, corresponding to the single value $|\xi h| = \pi$

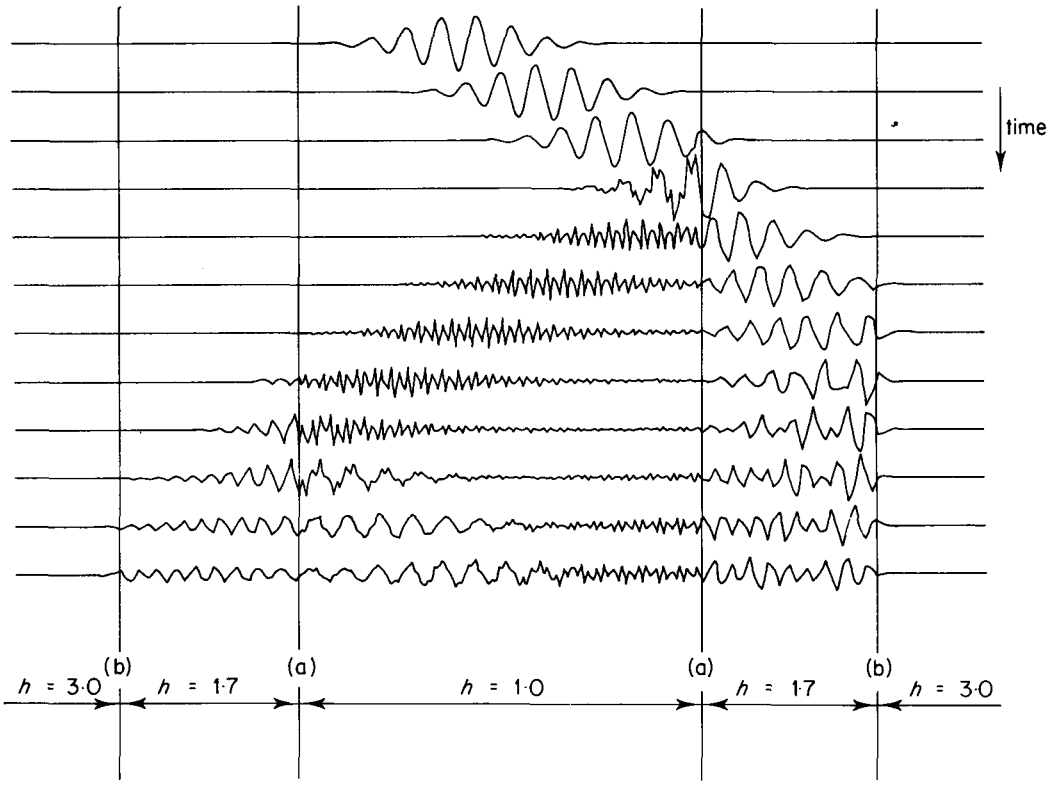

Figure 20. Same case as that given in Figure 19, except for the fact that the mesh size variations are not continuous but are implemented as two steps, (a) from $h = 1$ to $h = 1{\cdot}7$ then (b) $h = 1{\cdot}7$ to $h = 3$. The partial reflection or scattering which is observed at the mesh interface points (a) would be absent if the mesh size variation were smoothly distributed between many points, as is the case in Figure 19

in Fourier space, and they must have the infinite group velocity (from equation (80)):

$$G_q(|\xi h| = \pi) = \lim_{\delta \to 0} \left[- \frac{c}{1 - 2\left(\frac{1}{2} - \delta\right)} \right] = - \infty. \tag{146}$$

Indeed, these solutions are precisely those described by (57)–(59). And, by (28) and (145), their phase velocity is zero.

Although they cannot be generated by initial conditions, they may be generated by mishandled boundary conditions. To observe their existence, we have created a perfectly reflecting downwind boundary by imposing

$$u^j_{\text{BOUNDARY}} = 0 \tag{147}$$

and correspondingly

$$\rho(\omega) = \frac{\overline{q}_{\text{BOUNDARY}}(\omega)}{\overline{p}_{\text{BOUNDARY}}(\omega)} = - 1. \tag{148}$$

Shown in Figure 21 is the corresponding solution, generated by the total reflection of a smooth rightgoing solution coming from D. The leftgoing solution that may be observed follows

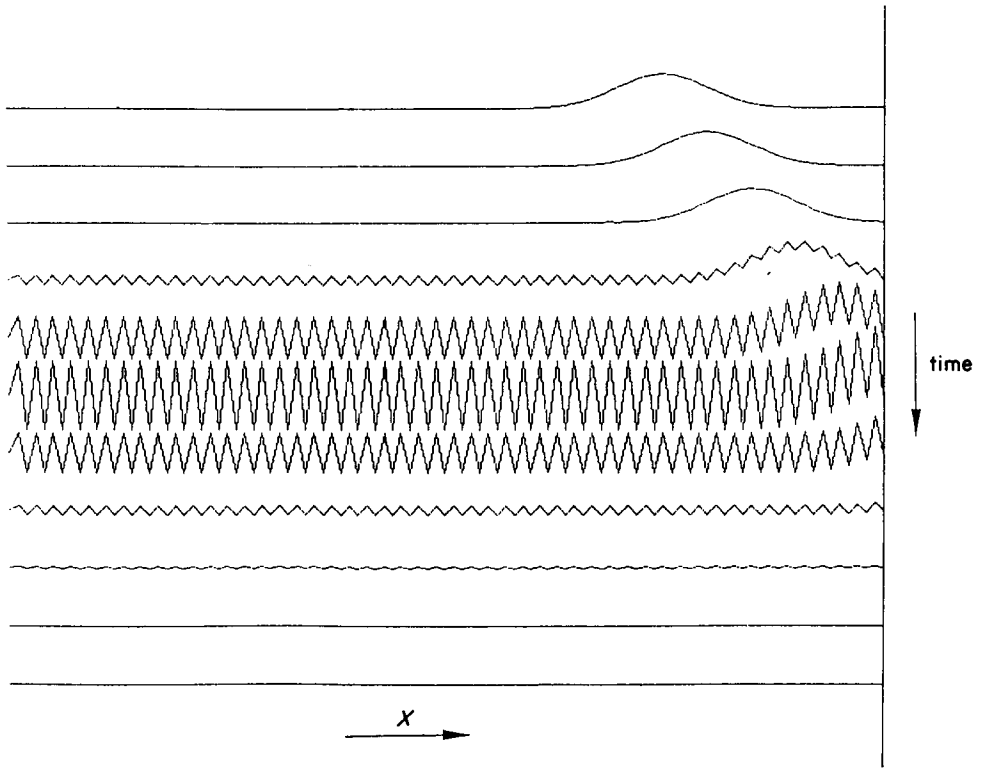

Figure 21. Generation of leftgoing solutions for the box method by the reflection of a smooth solution at an intentionally totally reflecting downwind boundary. Although the total $\mathscr{E}_\beta$ energy remains constant (and finite), the reflected l_2 energy is infinite. $R = 0{\cdot}5$. The absorbing boundary scheme (140) is used at the upwind (left) boundary

instantaneously its value generated at the boundary with a saw-toothed wave having a constant, horizontal envelope extending to $-\infty$.

A consequence of (148) and of the symmetry property of the characteristic admittance (section 7) is that the incident and reflected energy flows are equal and that therefore the total ($\mathscr{E}_\beta$) energy remains constant during reflection.

On the other hand, the fact that the reflected solution is of finite amplitude and infinite group velocity implies an infinite flow of reflected l_2 energy.

Although (147) is of course an intentional mishandling of the boundary that can be avoided in practice, the fact that the corresponding l_2 energy reflection ratio is infinite is indicative of the danger of large amounts of spurious noise that may occur in actual computations.

An example of this is given by the case illustrated in Figure 22: the simple two-point scheme

$$Mu_0^j = -c\left(\frac{u_0^j - u_{-1}^j}{h}\right) \tag{149}$$

is used at the downwind boundary instead of the natural scheme (131), for a computing domain where the box method applies. As may be observed, this consistent scheme generates a reflected solution of q type, when a smooth solution passes through the boundary, whereas (131) does not.

The analytic investigation of this problem may be conducted as before: Fourier transforming

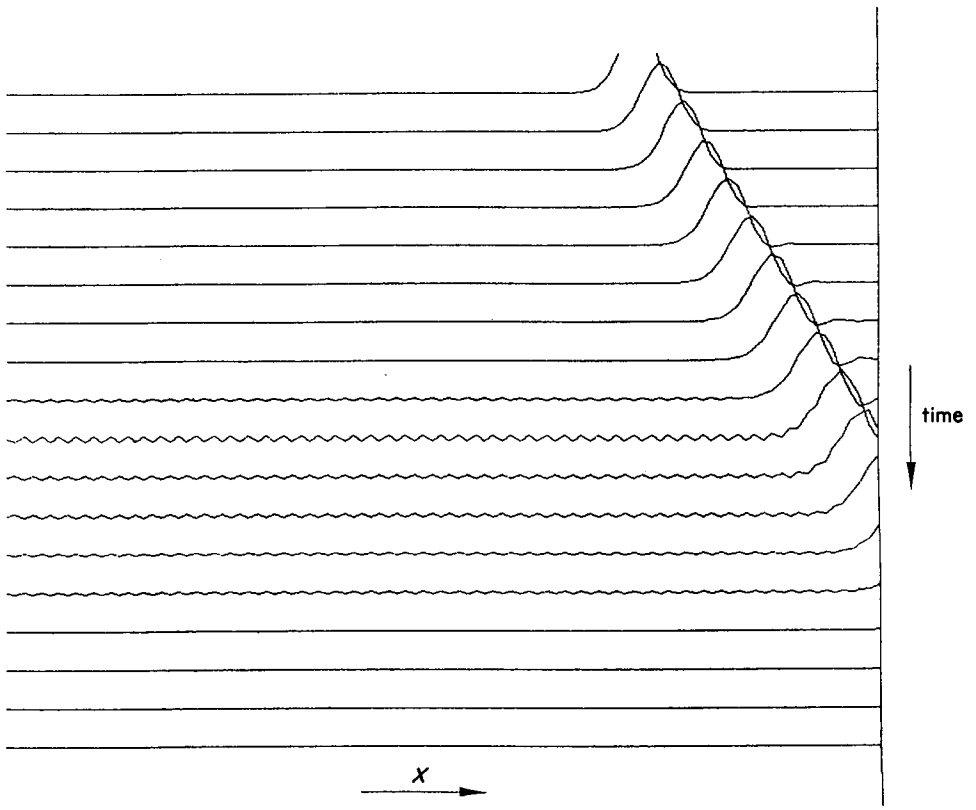

Figure 22. Reflection (in the form of a solution of q type with its characteristic saw-toothed appearance) at the downwind boundary of a domain in which the box method is used with the boundary scheme (149). The group velocity of the reflected solution is infinite, thus resulting in an infinite amount of l_2 energy leaving the boundary. The absorbing boundary scheme (140) is used at the upwind (left) boundary

equation (149) and solving for $\rho \equiv \overline{q}_0(\omega)/\overline{p}_0(\omega)$ results in the amplitude reflection ratio:

$$\rho(\omega) = -\frac{(\bar{\mu}/2)^2}{1+(\bar{\mu}/2)^2} \tag{150}$$

(Figure 23). The fact that (150) is finite and that the group velocity $G_q(\omega)$ is infinite means that an incident solution of finite l_2 energy at the boundary will generate a reflected solution of infinite l_2 energy, whence instability in the l_2 norm.

The interpretation of stability theories for initial-boundary value problems in terms of group velocity and energy flows is due to Trefethen,[18–20] in one of the most elegant applications of the concept of wave propagation to the analysis of boundary related questions. One of the standard conditions under which instability occurs is when *the boundary scheme has an infinite amplitude reflection ratio for some frequency* ω, resulting in the possibility of an infinite energy flow away from the boundary. The situation present here is different. What the combination of the box method and the boundary scheme (149) produces is *a finite amplitude reflection ratio with, for all frequencies, an infinite group velocity pointing away from the boundary*, also resulting in an infinite (l_2) energy flow away from the boundary. This new mode of instability is of course unique, owing to the singular property of the box method that admits solutions with an infinite group velocity.

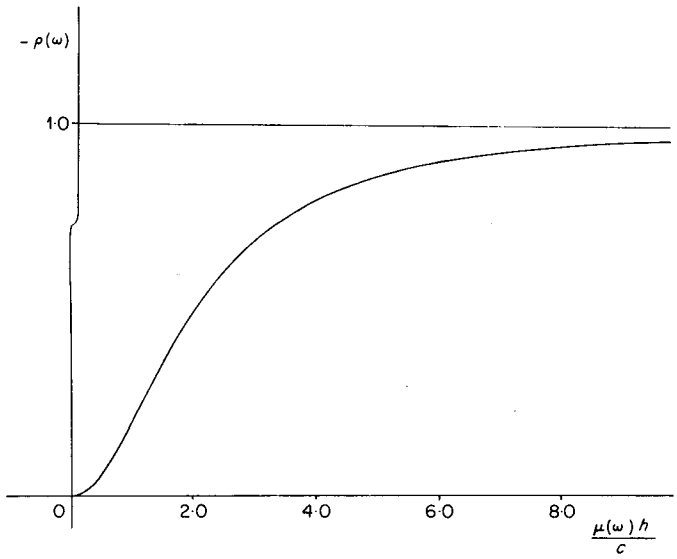

Figure 23. Amplitude reflection ratio of the boundary scheme (149) used at the downwind boundary of a computing domain in which the box scheme applies (equation (150))

A note about the numerical experiments of Figures 21 and 22: their description implies that the computing domain is limited by a downwind boundary at $x = 0$, and extends towards infinity to the left of that point. But the actual computing domain was of course finite:

$$D \equiv x \in [-L, 0] \tag{151}$$

as shown in Figures 21 and 22 and the boundary condition (140) was used at the upwind boundary $x = -L$. Since solutions of q type correspond to the single wave number $|\xi h| = \pi$ for the box method, and since (140) is perfectly absorbing for that wave number (equation (142)), the solution in (151) is as if this domain were extending to $-\infty$. The saw-toothed solutions (of q type) observed in Figures 21 and 22 have the interesting property of being of finite l_2 energy in D whereas the corresponding l_2 energy flow that they carry across $x = 0$ and $x = -L$ is infinite.

CLOSING REMARKS

The numerical approximation of partial differential equations creates errors which may be separated into two classes. The first is that of 'consistency errors'. Those are the errors which become vanishingly small when the mesh size is reduced, and which are considered in classical convergence theories. The second class of errors, which is particularly important with hyperbolic equations, contains what is best described as spurious solutions and they do not necessarily disappear when the mesh size tends to zero. It is in the analysis of this second class of errors that the wave propagation approach is particularly useful, as has been illustrated in this paper. We have examined from that perspective different occurrences of reflection at numerical boundaries, scattering at mesh refinement interfaces and internal reflection in non-uniform, slowly variable grids.

Wave propagation theory is closer to mathematical physics than to classical mathematics. It has been shown repeatedly that exploiting this close relationship with physics provides both the concepts and the semantics without which many of the observed spurious wave phenomena could not have been analysed.

The model equation and the computational algorithms considered in this paper have been relatively simple. But the basic concepts which have been described and analysed are more general, and the results suggest obvious applications to a wider range of problems in computational fluid dynamics.

REFERENCES

1. H. Lamb, *Hydrodynamics*, Cambridge University Press, 1932 (reprinted by Dover Publications, 1945).
2. T. Belytchsko and R. Mullen, 'On dispersive properties of finite element solutions', in I. Miklonitz and J. D. Achenbach (eds), *Modern Problems in Elastic Wave Propagation*, Wiley, New York, 1978.
3. B. Cathers and B. A. O'Conner, 'The group velocity of some numerical schemes', *Int. j. numer. methods Fluids*, **5**, 201–224 (1985). (Also: P. M. Gresho and R. L. Lee, Comments on "The group velocity of some numerical schemes", to appear in the same journal.)
4. R. C. Y. Chin, 'Dispersion and Gibbs phenomenon associated with difference approximations of initial-boundary value problems for hyperbolic equations', *J. Comp. Phys.*, **18**, 233–247 (1975).
5. R. C. Y. Chin, G. W. Hedstrom and K. E. Karlsson, 'A simplified Galerkin method for hyperbolic equations', *Math. Comp.*, **33**(146), 647–658 (1979).
6. M. G. G. Foreman, 'An analysis of two step time discretizations in the solution of the linearized shallow water equations', *J. Comput. Phys.*, **51**, 454–483 (1983).
7. W. G. Gray and G. F. Pinder, 'An analysis of the numerical solution of the transport equation', *Water Resources Research*, **12** (3), 547–555 (1976).
8. R. Grotjahn, 'Group velocity errors caused by finite differencing: a meteorological perspective', *Mathematics and Computer in Simulation.*, **27**, 37–46 (1985).
9. R. Grotjahn and J. J. O'Brien, 'Some inaccuracies in finite differencing hyperbolic equations', *Mon. Wea. Rev.*, 180–194 and 982 (1976).
10. H. L. Stone and P. L. T. Brian, 'Numerical solution of convective transport problems', *A.I.Ch.E. Journal*, **9**, 681–188 (1963).
11. R. Vichnevetsky, 'Propagation characteristics of semi-discretizations of hyperbolic equations', *Mathematics and Computers in Simulation*, **22**, 98–107 (1980).
12. G. Browning, H. O. Kreiss and J. Oliger, 'Mesh refinement', *Math. Comp.*, **27**, 29–39 (1973).
13. C. K. Chu and A. Sereny, 'Boundary conditions in finite difference fluid dynamic codes', *J. Comp. Phys.*, **15**, 476–491 (1974).
14. B. Engquist and A. Majda, 'Absorbing boundary conditions for the numerical simulation of waves', *Math. Comp.*, **31** (139), 629–651 (1977).
15. M. G. G. Foreman, 'An accuracy analysis of boundary conditions for the forced shallow water equations', *J. Comp. Phys.*, (1986).
16. L. Halpern, 'Absorbing boundary conditions for the discretization schemes of the one dimensional wave equation', *Math. Comp.*, **38** (158), 415–429 (1982).
17. I. Orlanski, 'A simple boundary condition for unbounded hyperbolic flows', *J. Comp. Phys.*, **21** (3), 251–265 (1976).
18. L. N. Trefethen, 'Wave propagation and stability for finite difference schemes', *Ph.D. Thesis*, Stanford University, 1982.
19. L. N. Trefethen, 'Group velocity of finite difference schemes', *SIAM Review*, **23**, 113–136 (1982).
20. L. N. Trefethen, 'Instability of difference models for hyperbolic initial boundary value problems', *Comm. Pure and Appl. Math.* **XXXVII**, 329–367 (1984).
21. R. Vichnevetsky, 'Propagation through numerical mesh refinement for hyperbolic equations', *Mathematics and Computers in Simulation*, **23**, 344–353 (1981).
22. R. Vichnevetsky, 'Propagation and spurious reflection in finite element approximations of hyperbolic equations', *Computers and Mathematics with Applications*, **11**, 733–746 (1985).
23. R. Vichnevetsky and E. C. Pariser, 'High order numerical Sommerfeld boundary conditions: theory and experiments', *Computers and Mathematics with Applications*, **11**, 67–78 (1985).
24. R. Vichnevetsky and E. C. Pariser, 'Non-reflecting upwind boundaries for hyperbolic equations', *Numerical Methods for Partial Differential Equations*, **2**, 1–12 (1986).
25. L. Wagatha, 'Approximation of pseudodifferential operators in absorbing boundary conditions for hyperbolic equations', *Numer. Math.*, **42**, 51–64 (1983).
26. P. M. Gresho, R. L. Lee and R. L. Sani, 'Advection dominated flows with emphasis on the consequences of mass lumping', in R. Gallagher *et al.* (eds), *Finite Elements in Fluids vol. 3*, Wiley, 1978 pp. 335–350.
27. J. M. Hyman, 'The method of lines solution of partial differential equations', *NYU report COO-3077-139*, 1976.
28. A. Papoulis *The Fourier Integral and its Applications*, McGraw-Hill, 1962.
29. R. Vichnevetsky and J. B. Bowles, *Fourier Analysis of Numerical Approximations of Hyperbolic Equations*, SIAM (in the Studies in Applied Mathematics series) Philadelphia, PA, 1982.
30. L. Brillouin, *Wave Propagation in Periodic Structures*, McGraw-Hill, New York, 1946.
31. J. J. Dronkers and J. C. Schonfeld, 'Tidal computations in shallow waters', *Proc. A.S.C.E.* **81**, (1955).

32. W. A. Miller, Jr., 'Numerical solution of the equations for unsteady open channel flow', *Ph.D. Thesis*, Georgia Inst. of Tech., 1971. Available through University Microfilms, Ann Arbor, Mich.
33. J. Lighthill, *Waves in Fluids*, Cambridge University Press, 1978.
34. V. Thomee and B. Wendroff, 'Convergence estimates for Galerkin methods for variable coefficient initial value problems', *SIAM J. Num. Anal.*, **11** (5), 1059–1068 (1974).
35. H. J. Pain, *The Physics of Vibrations and Waves*, 3rd edn, Wiley, 1983.
36. R. Vichnevetsky, 'Energy and group velocity in semi-discretizations of hyperbolic equations', *Mathematics and Computers in Simulation*, **23**, 333–343 (1981).
37. R. Vichnevetsky, 'Particle like properties of numerical wave propagation in irregular grids', *Report MAE 1714*, Princeton University, Mechanical and Aerospace Eng. Dept., 1985.
38. R. Vichnevetsky, 'Invariance theorems concerning reflection at numerical boundaries', *J. Comp. Phys.*, **63**, 268–282 (1986). (Also *Report MAE 1730*, Princeton University, Mechanical and Aerospace Eng. Dept.)
39. T. Matsuno, 'False reflection of waves at the boundary due to the use of finite differences', *J. Meteorological Soc. of Japan*, **44** (2), 145–157 (1966).
40. A. Jameson, W. Schmidt and E. Turkel, 'Numerical solution of the Euler equations by finite-volume methods using Runge–Kutta time stepping schemes', *AIAA Paper 81-1259*, 1981.
41. E. Turkel, 'Acceleration to steady state for the Euler equations', *ICASE Report No. 84-32*, NASA Langley Res. Center, 1984.
42. R. Vichnevetsky, 'Wave propagation and reflection in irregular grids for hyperbolic equations', *Applied Numerical Mathematics*, **2**, (1987). (Also: *Report MAE 1713*, Princeton University, Mechanical and Aerospace Eng. Dept)
43. H. Kreiss and J. Oliger, 'Methods for the approximate solution of time dependent problems', *Garp publication series no 10*, World Meteorological Organization, Geneva, 1973.
44. C. E. Grosch and S. A. Orszag, 'Numerical solution of problems in unbounded regions: coordinate transforms', *J. Comp. Phys.* **25**, 273–296 (1977).
45. M. B. Giles and W. T. Thompkins, Jr. 'Internal reflection due to a nonuniform grid', in R. Vichnevetsky and R. S. Stepleman (eds), *Advances in Computer methods for Partial Differential Equations V.* Pub. IMACS., 1984.
46. R. C. Y. Chin and G. W. Hedstrom, 'Scattering of waves from a staggered difference scheme on a variable grid', *Proc. 10th IMACS World Congress*, Montreal, Pub. IMACS., 1982.
47. G. B. Whitham, *Linear and Nonlinear Waves*, Wiley, 1974.
48. C. Cohen-Tadoudji, B. Diu and F. Laloe, *Quantum Mechanics* Wiley, 1977.
49. M. B. Giles and W. T. Thompkins, Jr. 'Propagation and stability of wavelike solutions of finite difference equations with variable coefficients', *J. Comp. Phys.*, **58**, 349–360 (1985).
50. G. W. Hedstrom, 'Models of difference schemes for $Ut + Ux = 0$ by partial differential equations', *Math. Comp.*, **29** (132), 969–977 (1975).
51. L. Lapidus and G. F. Pinder, *Numerical Solution of Partial Differential Equations in Science and Engineering*, Wiley, 1982.
52. R. Vichnevetsky, 'The energy flow equation', *Mathematics and Computers in Simulation*, **26**, 93–101 (1984).